



## RESEARCH ARTICLE

# Trigeminal neuropathy causes hypomyelination in the anterior cingulate cortex, disrupts the synchrony of neural circuitry, and impairs decision-making in male rats

Suresh K. Murugappan<sup>1</sup> | Mahadi Hasan<sup>1,2</sup> | Zhuogui Lei<sup>1,2</sup> | Zafar Iqbal<sup>1,2,3</sup> |  
Aruna S. Ramkrishnan<sup>1,2</sup>  | Heung Y. Wong<sup>1,2,3</sup> | Ying Li<sup>1,2,3,4</sup> 

<sup>1</sup>Department of Biomedical Sciences, College of Veterinary Medicine and Life Sciences, City University of Hong Kong, Kowloon, Hong Kong

<sup>2</sup>Department of Neuroscience, College of Veterinary Medicine and Life Sciences, City University of Hong Kong, Kowloon, Hong Kong

<sup>3</sup>Centre for Regenerative Medicine and Health, Hong Kong Institute of Science & Innovation, Chinese Academy of Sciences, Hong Kong SAR, P.R. China

<sup>4</sup>Centre for Biosystems, Neuroscience, and Nanotechnology, City University of Hong Kong, Kowloon, Hong Kong

## Correspondence

Ying Li, M.D., Department of Neuroscience,  
Department of Biomedical Sciences, City  
University of Hong Kong, Tat Chee Avenue,  
Kowloon, Hong Kong.  
Email: yingli@cityu.edu.hk

## Present address

Suresh K. Murugappan, Department of  
Biomedical Engineering, The Hong Kong  
Polytechnic University, Kowloon, Hong  
Kong

## Funding information

Innovation and Technology Fund;  
Research Grants Council, University  
Grants Committee, Grant/Award Number:  
11102820, 11100018, 11100914, 11166116,  
11101315 and 160713; City University  
of Hong Kong Centre for Biosystems,  
Neuroscience and Nanotechnology Grant,  
Grant/Award Number: 9360148; City  
University of Hong Kong Neuroscience  
Research Infrastructure Grant, Grant/  
Award Number: 9610211; Health and  
Medical Research Fund, Grant/Award  
Number: 05160256; NSFC-RGC Joint  
Research Scheme, Grant/Award Number:  
N\_CityU114/17; Shenzhen-Hong Kong  
Institute of Brain Science - Shenzhen  
Fundamental Research Institutions, Grant/  
Award Number: NYKFKT201912

## Abstract

Infraorbital nerve-chronic constriction injury (ION-CCI) has become the most popular chronic trigeminal neuropathic pain (TNP) injury animal model which causes prolonged mechanical allodynia. Accumulative evidence suggests that TNP interferes with cognitive functions, however the underlying mechanisms are not known. The aim of this study was to investigate decision-making performance as well as synaptic and large-scale neural synchronized alterations in the spinal trigeminal nucleus (SpV) circuitry and anterior cingulate cortex (ACC) neural circuitry in male rats with TNP. Rat gambling task showed that ION-CCI led to decrease the proportion of good decision makers and increase the proportion of poor decision makers. Electrophysiological recordings showed long-lasting synaptic potentiation of local field potential in the trigeminal ganglia-SpV caudalis (SpVc) synapses in TNP rats. In this study, TNP led to disruption of ACC spike timing and basolateral amygdala (BLA) theta oscillation associated with suppressed synchronization of theta oscillation between the BLA and ACC, indicating reduced neuronal communications. Myelination is critical for information flow between brain regions, and myelin plasticity is an important feature for learning. Neural activity in the cortical regions impacts myelination by regulating oligodendrocyte (OL) proliferation, differentiation, and myelin formation. We characterized newly formed oligodendrocyte progenitor cells, and mature OLs are reduced in TNP and are associated with reduced myelin strength in the ACC region. The functional disturbances in the BLA-ACC neural circuitry is pathologically associated with

Edited by Bradley Kerr, David McArthur, and Junie Warrington. Reviewed by Min Zhuo and Tie-Jun Shi.

This is an open access article under the terms of the Creative Commons Attribution-NonCommercial-NoDerivs License, which permits use and distribution in any medium, provided the original work is properly cited, the use is non-commercial and no modifications or adaptations are made.

© 2021 The Authors. *Journal of Neuroscience Research* published by Wiley Periodicals LLC

the myelin defects in the ACC region which may be relevant causes for the deficits in decision-making in chronic TNP state.

#### KEYWORDS

anterior cingulate cortex, brain network oscillations, decision-making, myelin plasticity, RRID: AB\_10861310, RRID: AB\_1141557, RRID: AB\_2231974, RRID: AB\_2534069, RRID: AB\_2536100, RRID: AB\_2629465, RRID: AB\_2832244, RRID: AB\_2890253, RRID: AB\_2890254, RRID: AB\_443473, RRID: SCR\_000012, RRID: SCR\_001622, RRID: SCR\_001818, RRID: SCR\_002798, RRID: SCR\_003070, RRID: AB\_1141521, spike-field phase locking, trigeminal neuropathic pain

## 1 | INTRODUCTION

Trigeminal neuropathic pain (TNP) is often accompanied by mechanical allodynia and hyperalgesia, and is usually difficult to treat by analgesics or surgical intervention. Studies have demonstrated that nociceptive neurons in the spinal trigeminal nucleus (SpV) display heightened responsiveness to afferent input (i.e., central sensitization) (Borsook et al., 2003; Latremoliere & Woolf, 2009; Sessle, 2005).

Available evidence suggests that electrical or natural noxious peripheral stimulation can potentiate strength at nociceptive synapses in the spinal cord (Latremoliere & Woolf, 2009). fMRI studies have revealed enhanced activation of the SpV, thalamus, and anterior cingulate cortex (ACC) in patients with TNP (Borsook et al., 2003; Witting et al., 2006), indicating the dysfunction of the brainstem sensory components and higher brain emotional-pain system. There has been no direct electrophysiological evidence of synaptic changes in the SpV and higher brain regions in the TNP state. In this study, we examined that the heightened synaptic glutamatergic transmission in the SpV may contribute to SpV sensitization and aggravate the symptoms of TNP.

It should be noted that the effects of enhancement of synaptic plasticity are not being filtered out or compensated at higher levels of the neuraxis. The ACC along with other regions, such as the insular cortex, has a crucial role in the processing of pain and the encoding of negative affect resulting in pain-related unpleasantness (Bliss et al., 2016; Talbot et al., 1991; Yan et al., 2012; Zhuo, 2019). Our previous studies have identified enhanced neuronal responses in the ACC to visceral stimulation in viscerally hypersensitive (VH) rats (Gao et al., 2006; Wang et al., 2015; Wu et al., 2008). ACC activation is critical for pain sensitivity (Cao et al., 2008; Fan et al., 2009) and long-term affective memory (Yan et al., 2012). Although ascending multisynaptic pathways from the trigeminal ganglion (TG) to the ACC have been identified (Iwata et al., 2011), there is no definitive study to demonstrate plasticity in the ACC neural circuitry in the chronic TNP state.

Human and animal studies suggest that chronic pain affects medial prefrontal cortex (mPFC)-related cognitive and emotional functions (Hart et al., 2000). Cognitive functions such as decision-making are dependent on the ACC, a subregion of the prefrontal cortex, raphe nucleus, lateral habenula, and amygdala (Hu, 2016; Mu et al., 2015; Rivalan et al., 2009; Shidara & Richmond, 2002;

### Significance

Orofacial neuropathic pain is difficult to treat by analgesics or surgical intervention. Electrophysiological studies show that rats with chronic trigeminal neuralgia exhibit dysfunctions of the brain's emotion-pain circuits. Myelination is critical for communication between brain regions, and myelin plasticity is an important feature for brain function. Chronic neuropathy causes demyelination in the brain and impairs vital cognitive functions such as decision-making. This work has major translational impact, suggesting a novel therapeutic avenue to target myelin-related cognitive deficits. For instance, regular exercise has considerable impact on myelin formation and consequently enhances executive functions such as learning, memory, and decision-making.

Zeeb & Winstanley, 2013). Chronic pain patients are impaired in the gambling-like situations such as the Iowa Gambling Task (Apkarian et al., 2004). To date, orofacial pain-related emotional and cognitive deficit and its underlying mechanisms have rarely been studied using experimental models. In this study, we used a rat gambling task (RGT) to evaluate the cognitive functions in rats with TNP, and demonstrated TNP-impaired decision-making in rats.

Systemic brain activity is rhythmic and interaction between distinct brain regions is essential for complex information processing. Large-scale neural oscillations are critical for modulating, filtering, and redirecting information flow in the network mechanisms in the brain (Colgin, 2013; Hu et al., 2020; Lu et al., 2016). Oscillations facilitate the synchronization of neurons, formation of cell assemblies (Buzsáki & Draguhn, 2004), and enhancement of adequate plasticity, subjecting to precisely timed pre- and postsynaptic activity (Markram et al., 1997). Through electrophysiological recordings in awake animals, we have shown that phase locking and synchronization within the ACC and between the ACC and basal lateral amygdala (BLA) are fundamental to the modulation of decision-making behavior in rats (Cao, Wang, Shahed, et al., 2016; Cao, Wang, Zhang, et al., 2016; Mu et al., 2015; Wang et al., 2017).

The myelination of the brain corresponds with cognitive and behavioral development (Hill et al., 2018). Being highly dynamic in nature, changes to myelin structure greatly affect brain plasticity and learning (Chang et al., 2016). As evidenced by human imaging studies, various types of learning coincide with structural modifications in the brain white matter (Zatorre et al., 2012). For example, professional musicians have been shown to have increased myelination in the white matter. In addition, studies in mice have demonstrated that changes in social and environmental conditions during a complex motor task can lead to modifications in oligodendrocytes (OLs) and myelination (McKenzie et al., 2014). The mechanism for myelin plasticity in cognitive performance remains largely unknown. Recent computational analysis suggests that the conduction delays between coupled oscillators in the brain can be sensitive to slight variations in conduction speed caused by minute changes in the myelin (Pajevic et al., 2014). Myelination accelerates axonal nerve impulse propagation, and hence facilitates long-range oscillations and synchrony of spike time arrival between neurons in different brain areas (Fields, 2015). Our recent studies using multiple paired association (PA) learning and memory paradigm showed that the establishment of memory patterns is associated with OL generation and adaptive myelination in ACC networks (Hasan et al., 2019).

Recently, it was proposed that abnormal myelin formation may contribute to a number of mental illnesses, including depression, schizophrenia, and bipolar disorders (Fields, 2008). The dysregulation of myelin plasticity may have serious consequences for neural network functioning. In this study, multiple electrode array recordings were performed in awake rats to characterize the CCI-induced alterations in the phase locking of ACC spikes to the phase of theta oscillations in the BLA (cross-area spike-LFP-phase locking) in the rats with chronic TNP. We hypothesize that infraorbital nerve (ION)-chronic constriction injury (CCI) leads to the dysregulation of myelin plasticity, and hypomyelination in ACC neuronal circuitry may have an adverse impact on neural network functioning. Hypomyelination is the causal mechanism underlying impaired decision-making in chronic pain state.

Microglia play a crucial role in neurodevelopment by interacting with neuronal cells such as OLs for wiring and neural circuit regulation (Thion et al., 2018). The elevated levels of pro-inflammatory cytokines, such as IL-1 $\beta$ , IL-6, and TNF- $\alpha$ , have been reported in patients suffering from chronic pain (Backonja et al., 2008; Costa et al., 2016) and experimental animal models with neuropathic pain (Apkarian et al., 2006; Xie et al., 2006). In this study, we revealed the role of microglial plasticity and pro-inflammatory cytokines in the chronic pain state.

## 2 | MATERIALS AND METHODS

### 2.1 | Animals

Experiments were performed in adult male Sprague-Dawley rats (300–350 g) which were housed in plastic cages in a standard

temperature and humidity-controlled room (25°C; 50% humidity) with 12-hr light/dark cycle, and they were given access to food and water ad libitum except for the period of the RGT. A total of 146 male animals were used in this study. Sex differences were not examined in this study. We acknowledge this as a limitation and all results should be interpreted with this information in mind. All animals were supplied by Laboratory Animal Services Centre, Chinese University of Hong Kong. All experimental procedures were carried out in accordance with the guidelines established by the National Institute of Health and approved by the Committee on the Use and Care of Animals at the City University of Hong Kong and the licensing authority for conduction of experiments, the Department of Health of Hong Kong (No.14-40 in DH/HA&P/8/2/5). Power analysis was not performed prior to start of the study to determine the sample size but are based on our previous publications (Cao, Wang, Mu, et al., 2016; Cao, Wang, Shahed, et al., 2016; Cao, Wang, Zhang, et al., 2016; Rivalan et al., 2009; Wang et al., 2017).

### 2.2 | Chronic trigeminal neuropathic pain model

Chronic constriction of the ION was performed to develop chronic TNP. The surgical procedures to ligate the ION were adapted from previous publication (Kernisant et al., 2008). Briefly, rats were anesthetized with an inhalant anesthetic (mixture of 3%–4% isoflurane and pure oxygen for medical usage). The skin above the eye was shaved and a curvilinear incision was made 2mm above the left eye along the curve of the frontal bone, and the muscle tissue close to the bone was then gently dissected laterally using a scalpel blade until the contents of the orbit could be gently retracted laterally. Once the eye was retracted, the ION was seen lying approximately 8-mm deep within the orbit on the maxillary bone. Five millimeter of the ION was gently freed from the surrounding connective tissue with fine jeweler's forceps and the two ligatures were then made 4-mm apart around the nerve using 5.0 chromic gut suture. After ligating ION, the incision above the eye was sutured and the rat was then kept undisturbed to recover. For sham-operated rats, similar surgical procedures were performed except that constriction of the ION was not performed.

### 2.3 | Allodynia and hypersensitivity testing

Mechanical pain sensitivity in the facial region was assessed as described in a previous publication (Kayser et al., 2010). Rats were stationed individually into a plastic cage to acclimatize to the testing environment. Mechanical sensitivity was assessed by applying the Von Frey filaments (VFF) between the whisker pad region and surgery site with VFF (Semmes-Weinstein monofilaments, Stoelting, Wood Dale, IL, U.S.A.) in an increasing force order that produced a bending force between 0.6 and 15.0 g until a brisk withdrawal response was triggered. VFF testing to assess mechanical allodynia in the facial region was performed 1 day before and 4, 7, 10, 15, 21, and 30 days after surgery.

## 2.4 | Rat gambling task

The experimental setup and procedures for the gambling task have been described in our earlier studies (Cao, Wang, Mu, et al., 2016; Cao, Wang, Shahed, et al., 2016; Cao, Wang, Zhang, et al., 2016; Rivalan et al., 2009; Wang et al., 2017). The rats were food restricted to 90% of their free-feeding weight during the entire RGT procedure. The rats were trained within a series of training sessions to associate nose-poke with the delivery of food pellet until attaining 100 pellets within 30 min. The number of nose-pokes per minute and the duration of the last training session were used to assess the general activity and motivation of the rats to perform the task.

The RGT was performed on Day 30 after surgery for the two experimental groups, namely sham-operated rats and ION-CCI rats. The entire test procedure lasted 60 min and was performed on the day after training completion. Rats were free to choose between the four apertures (A–D) as they were during the training phase; however, nose-pokes A and B led to larger immediate reward and higher time-out penalty, whereas nose-pokes C and D have lesser immediate reward and less penalty time-out, such that the rat continuously chooses nose-poke C or D will collect five times more food pellets than nose-poke A or B. The percentage of advantageous choices  $[(C + D)/(A + B + C + D) \times 100\%]$  chosen in the last 20 min was used as a criterion to distinguish the good (>70% advantageous choices), poor (<30% preference) decision makers, and undecided (30%–70% preference) (Cao, Wang, Mu, et al., 2016; Cao, Wang, Shahed, et al., 2016; Cao, Wang, Zhang, et al., 2016; Rivalan et al., 2009; Wang et al., 2017).

## 2.5 | Electrophysiological recordings

Single neuronal activity in the SpVc region is recorded using glass microelectrodes. For local field potential (LFP) recording, tungsten electrodes are positioned into the TG for stimulation and the responses from the SpVc region were recorded. Two 16-channel micro-wire electrode arrays (4 × 4) were inserted into the prelimbic area of the ACC and the ipsilateral BLA (Cao, Wang, Mu, et al., 2016; Cao, Wang, Shahed, et al., 2016; Cao, Wang, Zhang, et al., 2016; Hasan et al., 2019).

*Experiment 1.* Single unit recording of nociceptive neurons in SpVc caudalis (SpVc) response to orofacial mechanical stimulation.

For the single unit recording in the SpVc, the cisterna magna was opened. The overlying dura and subarachnoid membrane were removed. Single neuronal activity was recorded extracellularly using glass microelectrodes filled with 2 M sodium chloride, with resistances ranging from 20 to 40 M $\Omega$ . Extracellular single unit recordings were continuously performed while the electrode was gradually lowered through the caudal medulla and advanced into the SpVc part (1.5–2.0 mm posterior to the obex and 1.5–2.0 mm lateral to the midline) of the medulla at a 23°-degree angle in 1- $\mu$ m steps. The ground wire, fixed in the superficial brain surface distant from the recording electrode and secured to a screw on the skull, was connected to the amplifier. Signals were amplified, and band-pass

filtered as previous described (Wang et al., 2015). The orofacial regions, including whisker pad, and eyes were manually stimulated with a cotton-tipped probe and subsequently the signals were monitored on the oscilloscope and through audio speakers to confirm the signals were recorded from a neuron. The electrode was advanced until the action potential of a single discriminable neuron was detected in response to tactile stimulation. Noxious cutaneous stimulation was used sparingly so as to avoid damage to the skin and the production of peripheral sensitization. For nociceptive neurons, graded mechanical stimuli (15–60 g) were applied to the orofacial regions by the VFF, which were delivered in ascending order, each for 5 s at an interval >45 s. The responses of the tested neuron were recorded using the Axon instruments. The pressure-evoked responses of a given neuron were assessed by summing the number of spikes evoked by each of these graded stimuli.

*Experiment 2.* Evoked LFP recording of synaptic transmission in TG-SpVc pathway.

For the extracellular evoked LFP recording, another small hole (1–2 mm wide) was drilled in the skull above the TG (1.0–3.0 mm anterior to the bregma; 2.0–3.0 mm lateral to the midline) for placing a bipolar tungsten stimulating electrode. The electrode was mounted vertically in the manipulator and lowered into the brain at 100  $\mu$ m/min to ventral coordinate 9.0 mm relative to the surface of the dura. The stimulating electrode was then advances in 100- $\mu$ m steps until to contact bone or to a depth of 11.5 mm. A recording glass microelectrode (tip diameter 2–5  $\mu$ m, filled with 2.0 M NaCl, resistance of 1–4 M $\Omega$ ) was advanced into the SpVc in 1- $\mu$ m steps. After positioning the electrodes, the rat was left for 30 min before commencing the experiment. Test electrical stimuli (square wave pulse, duration: 0.2 ms, 30-s time interval) were delivered to the TG. The recording electrode was advanced into the SpVc until the maximal response to TG stimulus (400  $\mu$ A) was observed. Input-output (I/O) curves were generated by systematic variation of the stimulus current (from 200 to 1,000  $\mu$ A, in steps of 200  $\mu$ A) to evaluate synaptic strength. The TG was stimulated every 30 s and 10 stimuli were given at each current level; the evoked responses in the SpVc were digitized (10 KHz) and amplified (×100) by a high input impedance amplifier, and sent to a PC-based data acquisition system for online A/D conversion (Axon, Digidata 1440A) and digital analysis (Axoscope and Clampfit). The amplitude of the evoked field potential in SpVc was measured for the downward peak. The amplitudes of 10 responses recorded at each current level were averaged to construct the I/O curve.

To study the role of different glutamate receptors in this synaptic pathway, we performed pharmacological manipulations on TG-SpVc synaptic transmission *in vivo*, in separate groups of sham and ION-CCI rats. We performed reverse microdialysis into the SpVc of NMDA receptor antagonist aminophosphonopentanoic acid (AP5, 2.0 mM), AMPA/kainate receptor antagonist 6-cyano-7-nitroquinoxaline-2,3-dione (CNQX, 1.0 mM), or artificial cerebrospinal fluid at a rate of 2  $\mu$ l/min and subsequently recorded LFP signals in the SpVc at the same time. This technique allows the administration of drugs *in vivo* without affecting the tissue pressure or volume, and with no voltage or current stimuli. Detailed procedures were described in our previous study

(Wang et al., 2015; Wu et al., 2008). Microdialysis probes (Bioanalytical Systems, West Lafayette, IN, USA) with 3 mm of exposed membrane (320  $\mu\text{m}$  diameter,  $\sim 6,000$  Da permeability) were implanted into the SpVc (0.8 mm posterior to the obex and 1.0 mm lateral to the midline at  $30^\circ$ ) with a micromanipulator at  $5 \mu\text{m/s}$ . Recording microelectrodes were lowered into the SpVc about 2 mm lateral to the obex. The distance between the recording electrode and the tip of microdialysis probe was within 0.3–0.5 mm. In order to achieve stable electrophysiological recordings in rats undergoing reverse microdialysis, recordings started 2 hr after probe implantation. Basal synaptic transmission and I/O curve studies were performed as described above.

**Experiment 3.** Multiple channel electrophysiology recording in ACC and BLA.

Three weeks after the nerve ligation surgery or sham treatment, rats were anesthetized with intraperitoneal injection of urethane (i.p. 1.5 g/kg) and placed in a stereotaxic frame. Craniotomies (1–2 mm wide) were performed to expose the brain areas above the right side of the ACC (stereotaxic coordinates: anterior–posterior (AP) = 3.0–3.3, medial–lateral (ML) = 0.6–1.0, dorsal–ventral (DV) = 2.8–3.5 mm from the dura) and the ipsilateral BLA (AP –3.3 to –3.6, ML 5.0–5.3, depth 6.5–7.5 mm).

Microwires, constructed in four rows with four wires in each row (electrode diameter = 25  $\mu\text{m}$ ; electrode spacing = 250  $\mu\text{m}$ ; row spacing = 250  $\mu\text{m}$ ; impedance = 20–50 k $\Omega$ , measured with microelectrode meter  $\Omega$ mega-Tip Z, WPI instruments), were used in this study. One wire from each array was wrapped around one of the bone mounting screws to ground. LFPs and spike firing were recorded with a 64-channel electrophysiological data acquisition system (OmniPlex® D system, Plexon, Dallas, TX). LFPs were amplified ( $\times 20,000$ ), band-pass filtered (0.05–200 Hz, 4-pole Bessel), and sampled at 1 kHz. Spikes were identified when a minimum waveform reached an amplitude threshold of 4.5 standard deviations higher than the noise amplitude, and were filtered (300–5,000 Hz, 4-pole Bessel) and sampled at 40 kHz. Signals from the ACC and BLA were recorded simultaneously during 60-s spontaneous activity.

## 2.6 | Multiple channel electrophysiological data analyses

Data analyses were performed using a combination of tools in MATLAB, NeuroExplorer, and Offline Spike Sorter (Table 2). The detailed procedures of multiple channel data analyses have been described in our recent publications (Cao, Wang, Mu, et al., 2016; Cao, Wang, Shahed, et al., 2016; Cao, Wang, Zhang, et al., 2016; Hasan et al., 2019). Three rats were excluded from this study due to the misplacement of the electrodes ( $n = 3$ ).

### 2.6.1 | Power spectral analysis

The power spectral density of the LFPs recorded in the ACC region was analyzed. The raw LFPs of ACC were filtered between 1 and

20 Hz using fourth-order Butterworth. The band power was defined as the area under the curve of the corresponding frequencies, and the band power from each animal was averaged over the 16 channels in the ACC.

### 2.6.2 | Spike sorting

Single unit spike sorting was done using Offline Spike Sorter software (Version 4, Plexon Inc.). A single unit was identified using the criterion of finding  $<3\%$  of the spikes in the refractory period of 2ms in the interspike interval (ISI) histograms. Detailed procedures have been described in our recent publications (Cao, Wang, Mu, et al., 2016; Cao, Wang, Shahed, et al., 2016; Cao, Wang, Zhang, et al., 2016; Mu et al., 2015).

### 2.6.3 | Spike-field coherence

SFC between the spikes recorded in the ACC and the averaged LFP from the BLA was quantified. Only neurons with at least 50 spikes during the period analyzed were used for SFC analysis. For every spike, a segment of the LFP data centered on the spike  $\pm 480$  ms long was extracted. The spike-triggered average (STA) was calculated as the mean of all these sections. Then, the frequency spectrum of the STA (fSTA) was calculated using MATLAB functions for multitaper analysis. The average of these individual frequency spectra resulted in the spike-triggered power as a function of frequency STP(f). Finally, the SFC was calculated as the fSTA over the STP(f) as a percentage.  $\text{SFC}(f) = [\text{fSTA}(f)/\text{STP}(f)] * 100\%$ .

### 2.6.4 | Phase locking of single neuron spikes to the theta oscillation

We plotted the phase distribution and analyzed the Rayleigh test using custom-written MATLAB scripts (Rutishauser et al., 2010) to study the angular distribution of ACC spikes in relation to the ongoing BLA theta oscillation to help clarify the strength of phase locking. To ensure the validity of the statistical results, only neurons with at least 50 spikes during the period analyzed were used for phase-locking estimation. A neuron was considered phase locked in the theta range if the p-value was below the threshold of 0.0023.

### 2.6.5 | Synchronized theta oscillations between ACC and BLA by cross-correlation analyses

The synchronized theta LFP activities between ACC and BLA were evaluated by computing cross-correlograms. Theta-filtered LFPs from the ACC and BLA were aligned, and the LFP in the ACC was chosen as the reference. Pearson correlation coefficients were calculated with a lagging time ranging from –0.5 to 0.5 s with small bins



(2 ms). The cross-correlation curves were smoothed with a Gaussian filter. The cross-correlograms from valid electrode channels in the ACC and BLA were analyzed for the second positive peak located around 0.2-s lagging time as a quantitative measure which represents theta activity at about 5 Hz.

## 2.7 | Immunohistochemistry

On Day 30 after ION-CCI surgery, mechanical stimulation is applied on the orofacial region and the rats were euthanized within 90 min after the mechanical stimuli by transcardial perfusion of paraformaldehyde. The brain samples were collected for immunostaining procedures. The brain was postfixed in 4% PFA overnight at 4°C. Tissue were cryoprotected in 30% sucrose before freezing in OCT. Next, 30- $\mu$ m slices of the brain were collected and processed as floating slices. The brain sections containing region corresponding to the ACC (sections from 3.8 to 2.2 mm from the bregma) were collected for immunohistochemistry. Primary antibodies were diluted in blocking solution (0.1% [v/v] Triton X-100 and 10% goat serum in 0.01 M PBS) and was applied to slices overnight at 4°C. Then slices were washed and incubated for 2 hr with secondary antibodies. The following primary antibodies were used in this study: (i) rabbit anti-myelin basic protein (anti-MBP; 1:500, Abcam Cat# ab40390, RRID:AB\_1141521); (ii) Mouse anti-NG2 (1:500, Abcam Cat# ab177025, RRID: AB\_2890253), (iii) Mouse anti-APC (CC1; 1:500, Abcam Cat# ab16794, RRID:AB\_443473), (iv) Rabbit anti-c-Fos (1:500, Synaptic Systems Cat# 226 003, RRID:AB\_2231974), (v) Rabbit anti-Olig2 (1:500, Abcam Cat# ab109186, RRID:AB\_10861310), (vi) Rabbit anti IBA1 (1:500, Abcam Cat# ab178847, RRID:AB\_2832244), (vii) Mouse anti-CD68 (1:500, Abcam Cat# ab31630, RRID:AB\_1141557), and (viii) Mouse anti-IL1 $\beta$  (1:500, Abcam Cat# ab156791, RRID:AB\_2890254) (Tables 1 and 2). MBP antibodies stain the MBP proteins in the myelin fibers; NG2 antibodies stain the neuron-glia antigen 2 (NG2) present in the surface of oligodendrocyte progenitor cells (OPC); CC1 antibodies stain the cell body of the mature OLs; and c-Fos is an immediate early gene expression protein that used to increase following neural activity. IBA1 is a microglial marker that marks the microglial cells; CD68 and IL-1 $\beta$  are pro-inflammatory cytokines markers that stains the expression of cytokines. Finally, slices were mounted on slides and imaged by using an inverted laser scanning confocal microscope (LSM 880, Carl Zeiss). A total of three to five sections were examined per rat, and five or six rats were analyzed per sham and ION-CCI group. Confocal images represent projected stacks of 10 images collected at 1- to 2- $\mu$ m steps. The intensity of MBP+ myelin was measured up to 1,000  $\mu$ m from the pial surface (midline) covering layers I–VI in the ACC region. The intensity of MBP+ myelin was calculated using ImageJ (RRID:SCR\_003070). The MBP+ myelin intensity was normalized with the sham-operated control samples. The number of NG2+ cells and CC1+ cells were also calculated within the field of view containing layers I–VI of the ACC region in triplicates for each experimental group. Layer I is close to the midline separating the

cerebral hemispheres and Layer VI should be around 1000 $\mu$ m from the midline. Three independent experiments were performed. The counting of cells were done by two persons blinded to the experimental groups and then averaged.

## 2.8 | Transmission electron microscopy

Transmission electron microscopy (TEM) was conducted by following our previous established method (Hasan et al., 2019). Briefly, rats were perfused with 0.1 M PB followed by 2% glutaraldehyde/ 4% PFA in sodium cacodylate buffer. A block of approximately 1  $\times$  1  $\times$  2 mm<sup>3</sup> from the right ACC was dissected out and then postfixed with the primary fixative, then contrasted with 1% osmium tetroxide (vol/vol) in PBS. Tissues were dehydrated in an ethanol graded from 50% to 100% and embedded in Epon. Ultrathin slices (80 nm) were cut and stained with 2% uranyl acetate (vol/vol) and Reynolds' lead citrate, and analyzed with TEM.

## 2.9 | Western blot analysis

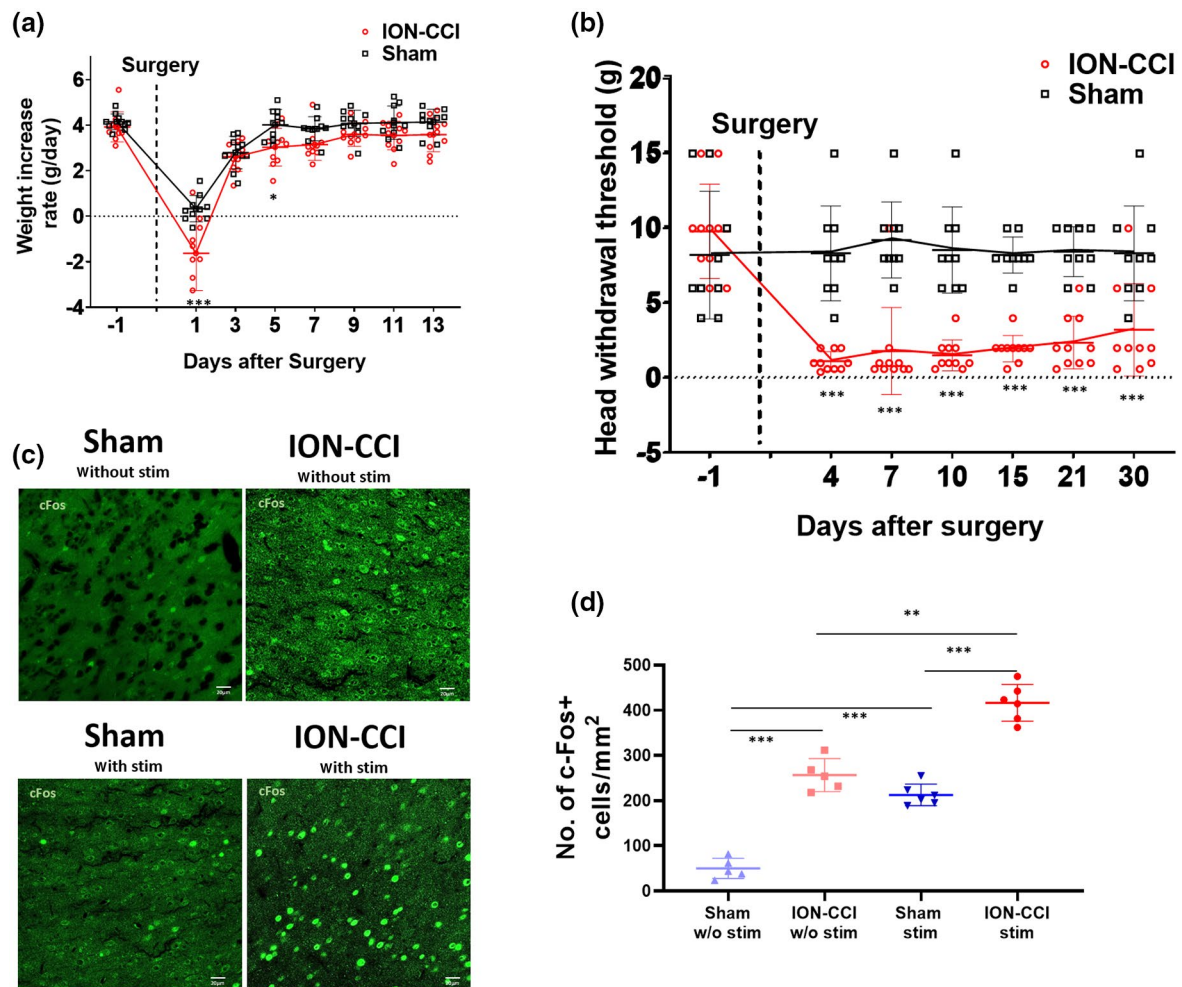
Western blot analysis was performed from brain lysate collected from the ACC, using the protocol from our previously published paper (Hasan et al., 2019). Briefly, rats were acutely anesthetized with urethane (1.5 g/kg), and then the brains were quickly detached and placed into ice-cold PBS. Brains were sectioned on an anodized aluminum brain slicer (Braintree Scientific Instruments). Then, bilateral ACCs were identified, dissected, and were homogenized in ice-cold radioimmunoprecipitation assay total protein extraction buffer (50 mM Tris, 150 mM NaCl, 1% NP-40, 0.5% sodium deoxycholate, 0.1% sodium dodecyl sulfate) containing 1 mM phenylmethylsulfonyl fluoride and protease inhibitor cocktail (Roche). Homogenates were placed on ice for 15 min and centrifuged at 15,000 g for 30 min at 4°C and the supernatant was extracted as total protein for Western immunoblot analysis. The total protein content of each brain homogenate lysate is determined by Bio-Rad DC protein assay Kit. Ten micrograms of proteins was separated using SDS-PAGE and then transferred onto a polyvinylidene fluoride membrane (Bio-Rad, 0.2  $\mu$ m pore size). The membrane containing the proteins was blocked in 5% non-fat milk in a buffer of Tris-Buffered Saline containing 0.1% Tween 20 (TBST buffer). The membranes were then incubated for 16 hr overnight at 4°C with various primary antibodies diluted in blocking buffer. The membranes were then incubated with horseradish peroxidase-conjugated secondary antibodies diluted in blocking buffer (1:10,000), for 1 hr at room temperature. Western blots images were obtained using a Gel Documentation system (Azure Biosystems). The anti-MBP, anti-IL1  $\beta$ , anti-CD68, and anti- $\beta$  actin (ImmunoWay Cat# YM3028, RRID: AB\_2629465) antibodies were used at the indicated dilution of 1:5,000. The intensity of bands was quantified with ImageJ and normalized with  $\beta$  actin. The experiment was conducted three independent times (Tables 1 and 2).

TABLE 1 Key resource identifiers of antibodies used for immunostaining and Western blot experiments

Antibody	RRID	Host species	Clonality	Immunogen	Manufacturer	Dilution used
Rabbit anti-MBP	AB_1141521	Rabbit	Polyclonal	Synthetic peptide corresponding to mouse myelin basic protein aa 150 to the C-terminus conjugated to keyhole limpet hemocyanin	Abcam (Cat# ab40390)	1:500 (for IHC) 1:5,000 (for WB)
Mouse anti-NG2	AB_2890253	Mouse	Monoclonal	Clone 132.38 corresponding to NG2	Abcam (Cat# ab177025)	1:500 (for IHC)
Mouse anti-APC (CC1)	AB_443473	Mouse	Monoclonal	Synthetic peptide corresponding to APC aa 1-226	Abcam (Cat# ab16794)	1:500 (for IHC)
Rabbit anti-c-Fos	AB_2231974	Rabbit	Polyclonal	Synthetic peptide corresponding to aa 2 to 17 from rat c-Fos	Synaptic Systems (Cat#226003)	1:500 (for IHC)
Rabbit anti-Olig2	AB_10861310	Rabbit	Monoclonal	Synthetic peptide	Abcam (Cat# ab109186)	1:500 (for IHC)
Rabbit anti-IBA1	AB_2832244	Rabbit	Monoclonal	Synthetic peptide	Abcam (Cat# ab178847)	1:500 (for IHC)
Mouse anti-CD68	AB_1141557	Mouse	Monoclonal	Corresponding to CD68 rat spleen cell	Abcam (Cat# ab31630)	1:500 (for IHC) 1:5,000 (for WB)
Mouse anti-IL-1 $\beta$	AB_2890254	Mouse	Monoclonal	Recombinant full-length protein corresponding to human IL-1 beta aa 1-300	Abcam (Cat# ab156791)	1:500 (for IHC) 1:5,000 (for WB)
Mouse anti- $\beta$ actin	AB_2629465	Mouse	Monoclonal	Synthetic Peptide of $\beta$ -actin	ImmunoWay (Cat# YM3028)	1:5,000 (for WB)
Alexa Fluor 488 goat anti-mouse IgG H + L	AB_2534069	Goat	Polyclonal		Thermo Fisher Scientific (Cat# A-11001)	1:500 (for IHC)
Alexa Fluor 555, Goat anti-Rabbit IgG (H + L)	AB_2536100	Goat	Recombinant Polyclonal		Thermo Fisher Scientific (Cat# A-27039)	1:500 (for IHC)

TABLE 2 Research resource identifiers of reagents and software used for experiments and analysis

Reagents and Software	Resource identifier	Source
BCA Protein Assay Kit	Cat# 23225	Thermo Fisher Scientific
Tissue-Tek OCT Compound	Cat# 4583	Sakura
DAPI	Cat# D1306	Thermo Fisher Scientific
PVDF membrane	Cat# 1620177	BioRad
Prism 8.0	SCR_002798	GraphPad Software
ImageJ (version 1.53a)	SCR_003070	National Institutes of Health
NeuroExplorer	SCR_001818	Plexon Inc.
Offline sorter	SCR_000012	Plexon Inc.
MATLAB	SCR_001622	MathWorks



**FIGURE 1** Mechanical nociceptive pain behavior in ION-CCI and sham rats. (a) The rate of body weight increase in ION-CCI and sham-operated rats for 13 days following surgery. Statistical significance was determined by two-tailed unpaired *t*-test. \* $p < 0.05$ , \*\*\* $p < 0.001$ . (b) Time course of changes in the head-withdrawal threshold to mechanical stimulation of the orofacial skin region ipsilateral to the constricted nerve site in sham rat and ION-CCI rat. Results are presented as mean  $\pm$  SD,  $n = 9$  for sham group and  $n = 10$  for ION-CCI group. Statistical significance was determined by two-tailed unpaired *t*-test. \*\*\* $p < 0.001$ . (c) Representative micrograph of c-Fos expression in the ACC labeled by neuronal nuclei (NeuN) (layer I to IV, sections from 2.2 to 3.8 mm from the bregma). c-Fos (green)-stained coronal section shows the laminar distribution of excited cells in response to mechanical stimuli in ION-CCI and sham rats. Scale bar, 20  $\mu$ m. (d) No. of c-Fos+ cells in the ACC of ION-CCI and sham rats after orofacial stimulation and without stimuli. More c-Fos+ cells that are observed in ION-CCI rats indicate higher activation in response to mechanical stimuli compared to that of sham rats. Results are presented as mean  $\pm$  SD SEM,  $n =$  five or six rats per group. Statistical significance was determined by two-tailed unpaired *t*-test. \*\* $p < 0.01$ , \*\*\* $p < 0.001$



## 2.10 | Statistical analysis

Data are expressed as mean  $\pm$  SD, and statistical significance analyzed with GraphPad Prism v7.0 (GraphPad, CA) or SPSS 24.0 (Chicago, IL, USA). SPV electrophysiological data and VFF pain sensitivity were analyzed with two-way factorial ANOVA analysis followed by Bonferroni's post hoc tests for multiple comparisons. The data with normal distribution with mean and variance of two groups were analyzed with two-tailed unpaired *t*-test. A value of  $p < 0.05$  was considered statistically significant for all comparisons, except for Rayleigh's test where  $p < 0.0023$  (0.05/ 22 frequencies tested) was considered significant phase locking. The data showing the proportion of decision makers is presented in ordinal coordinates with a nonnormal distribution; therefore, a Mann-Whitney U test was performed to assess significance.

## 3 | RESULTS

### 3.1 | Mechanical nociceptive behavior

Both ION-CCI and sham rats showed a decrease in body weight gain for 3 days following surgery after which their body weight gain is recovered to presurgery body weight increase rate. On Day 13 after surgery, there was no significant difference in body weight increase rate in ION-CCI rats compared to that of sham rats (Figure 1a;  $F_{1,18(\text{surgery})} = 0.1823$ ,  $p = 0.6745$ ,  $F_{7,126(\text{time})} = 85.43$ ,  $p < 0.001$ ,  $F_{7,126(\text{interaction})} = 2.803$ ,  $p = 0.0096$ , two-way ANOVA repeated-measures post hoc Bonferroni test). The mechanical threshold to orofacial stimulation in the sham-operated rats remained in the similar range as the presurgery baseline. In contrast, ION-CCI surgery markedly decreased the mechanical pain threshold in the ipsilateral side of the facial region, with the difference in pain threshold first being detected on the fourth day and peaking in the first week. The ION-CCI pain sensitivity was significantly higher than that of sham (Figure 1b;  $F_{1,17(\text{surgery})} = 41.93$ ,  $p < 0.001$ ,  $F_{6,102(\text{time})} = 11.12$ ,  $p < 0.001$ ,  $F_{6,102(\text{interaction})} = 13.06$ ,  $p < 0.001$ , two-way RM-ANOVA post hoc Bonferroni test) and remained so at least for 30 days. These results are consistent with previous reports suggesting that ION-CCI surgery in rats evokes pain which is severe in the first week and causes mechanical allodynia for at least 120 days (Vos et al., 1994).

### 3.2 | c-Fos activation in response to mechanical stimulation

To identify the ACC neuronal activity in response to mechanical pain threshold in the ipsilateral side of the facial region, we performed immunohistochemistry to identify immediate early gene c-Fos expression. c-Fos is immediate early gene whose expression can be used as a neuronal activity marker and found to be increased after spinal (Hossaini et al., 2010) and orbitofrontal cortex (Leite-Almeida et al., 2014) in neuropathic rat models. The c-Fos expression of cells

in the ACC region was significantly elevated in both groups following mechanical stimulation (stim). ION-CCI rats show higher expression of c-Fos cells compared to sham rats (Figure 1c,d;  $256.8 \pm 36.4$  c-Fos cells/mm<sup>2</sup> for ION-CCI rats versus  $50.2 \pm 22.2$  for sham rats;  $n = 5$  rats per group,  $t_8 = 10.81$ ,  $***p < 0.001$ ). Mechanical stimulation elevated the c-Fos expression in ION-CCI rats to  $416.6 \pm 40.7$  c-Fos cells/mm<sup>2</sup> from  $256.8 \pm 36.4$  c-Fos cells/mm<sup>2</sup> ( $n = 6$  ION-CCI rats with stim and  $n = 5$  ION-CCI rats without stim,  $t_9 = 6.794$ ,  $***p < 0.001$ ). Sham rats after mechanical stimulation elevated the c-Fos expression to  $212.9 \pm 24.0$  c-Fos+ cells/mm<sup>2</sup> from  $50.2 \pm 22.2$  c-Fos+ cells/mm<sup>2</sup> observed in nonstimulated sham rats (Figure 1d;  $n = 6$  sham rats with stim and  $n = 5$  sham rats without stim,  $t_9 = 11.51$ ,  $***p < 0.001$ ). c-Fos is expressed in both sham and ION-CCI rats following mechanical stimulation, but the c-Fos expression is significantly higher in ION-CCI rats (Figure 1d;  $416.6 \pm 40.7$  c-Fos cells/mm<sup>2</sup> for ION-CCI rats with stim versus  $212.9 \pm 24.0$  for sham rats with stim;  $n = 6$  rats per group,  $t_{10} = 10.55$ ,  $***p < 0.001$ ). The increase in c-Fos expression in the ACC region in ION-CCI indicates that spontaneous pain activates the cells in the higher brain regions.

### 3.3 | Decision-making deficit in ION-CCI rats

RGT was performed to assess the decision-making abilities of the rats in a complex, conflicting environment. Two control rats and two CCI rats developed a selection bias of spatial preference for one specific nose-poke or side (two preferred left side and two right) during training and 60-min test, and were excluded from the final analysis. The responses during the last training session show that there was no significant difference in the general activity (Figure 2a;  $t_{42} = 1.183$ ,  $p = 0.2436$ , unpaired Student *t*-test) and motivational level (Figure 2b;  $t_{42} = 1.238$ ,  $p = 0.223$  unpaired Student *t*-test) between sham rats ( $n = 22$ ) and ION-CCI rats ( $n = 22$ ). This is consistent with previous studies showing that neuropathic pain does not affect the general eating and locomotor activity in the cage (Vezzani & Viviani, 2015), suggesting that ION-CCI surgery does not affect basal motor function and motivation for collecting food. ION-CCI rats collected fewer food pellets during the test session compared to sham rats (Figure 2c;  $t_{42} = 4.808$ ;  $p \leq 0.001$ ;  $n = 22$  rats for sham and 22 rats for ION-CCI rats, unpaired Student *t*-test).

Three types of decision makers were observed in sham and ION-CCI groups: good decision makers, poor decision makers, and undecided decision makers during the RGT, as defined by their preference for nose-pokes C and D. The dynamic pattern of choosing advantageous nose-pokes C and D over disadvantageous nose-pokes A and B during the entire testing period was noted in ION-CCI group (Figure 2e) and sham group (Figure 2d). During the course of the RGT, the proportion of choosing advantageous choices in the good and poor decision-making rats was clearly distinct from the chance level (50%) (Figure 2d,e,  $*p < 0.05$ ,  $**p < .01$ ,  $***p < .001$ , one-sample *t*-test) within the group and the characteristics of good decision makers in both sham and ION-CCI group were similar, that is the rats tend to choose the advantageous nose-pokes consistently

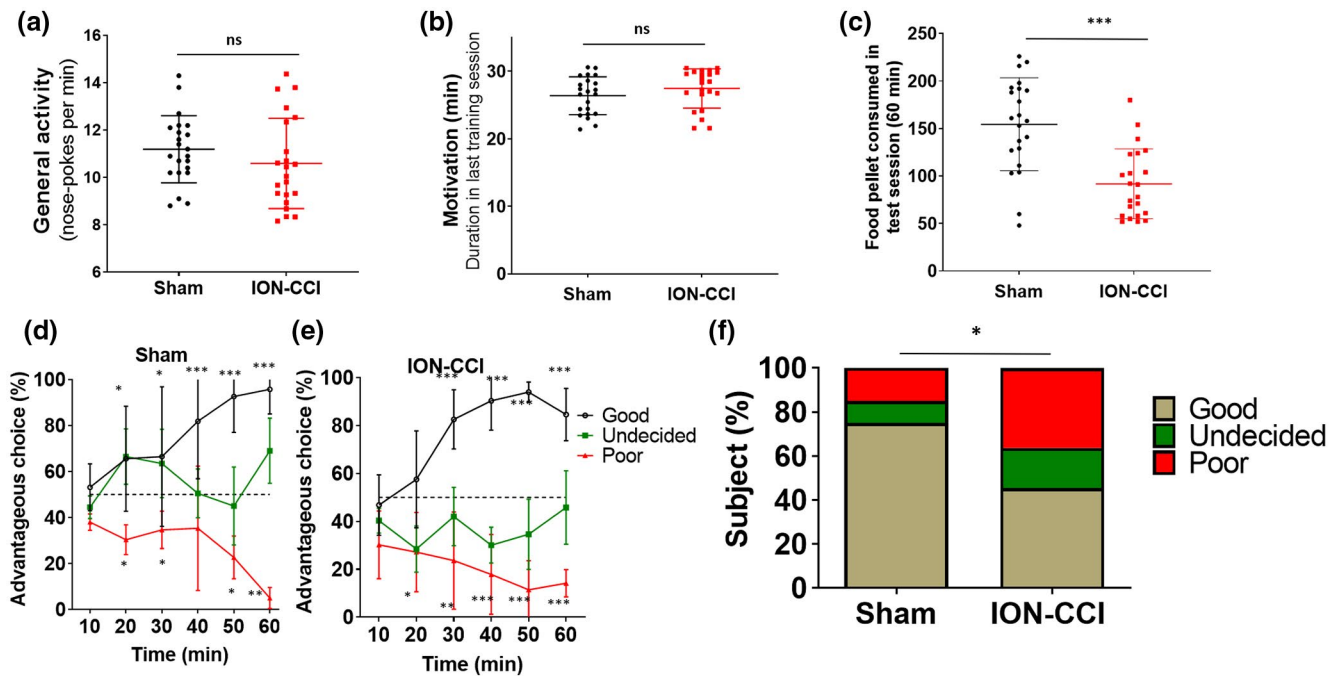


**FIGURE 2** Assessment of decision-making behavior in ION-CCI and sham rats. (a) General activity measured as the total number of nose-pokes made per minute. No significant difference was detected in the general activity in the sham and ION-CCI as determined by two-tailed unpaired *t*-test. n.s.,  $p > 0.05$ . (b) Motivation is measured as the duration taken to consume 100 food pellets during the last T2 training session. Motivation level is maintained at an optimum level for each rat before RGT. All the rats were equally motivated for the task and there is no significant difference in the motivation levels between the two groups as determined by two-tailed unpaired *t*-test. n.s.,  $p > 0.05$ . (c) The food pellets obtained during the test for sham and ION-CCI rats. Results are presented as mean  $\pm$  SD,  $n = 22$  for sham and  $n = 22$  for ION-CCI rats, \*\*\* $p < 0.001$ ; two-tailed unpaired *t*-test. (d) Time course of choosing advantageous choices among good, undecided, and poor decision makers during the RGT observed in sham rats. The choices that are statistically different from chance level (50%) was determined by one sample *t*-test, \* $p < 0.05$ , \*\* $p < 0.01$ , \*\*\* $p < 0.001$ ; one sample *t*-test. (e) Time course of choosing advantageous choices among good, undecided, and poor decision makers during the RGT observed in ION-CCI-operated rats. \* $p < 0.05$ , \*\* $p < 0.01$ , \*\*\* $p < 0.001$  versus 50% (chance level); one sample *t*-test. (f) The rats in each group were divided into three types of decision makers based on the choices during the last 20 min of the task. The different proportions of the three types of decision makers in ION-CCI rats ( $n = 22$ ). Statistical significance between three types of decision makers in sham and ION-CCI rats was determined by Mann-Whitney U test

in the 30- to 60-min period. Also, the characteristics of poor decision makers in both groups were similar. However, the proportion of good and poor decision makers was different in each group. ION-CCI rats were significantly different from sham-operated rats (Figure 2f;  $n = 22$  rats per group;  $U = 163$ ,  $Z = 1.843$ ,  $p = 0.033$ , Mann-Whitney U test). Sham-operated rats had a greater proportion of good decision makers (77.3%) and a smaller number of poor decision makers (13.6%) and undecided decision makers (9.1%) (Figure 2f). In ION-CCI rats, the proportion of good decision makers was reduced (45.5%) and the number of poor decision makers was increased (36.4%) compared to that of sham rats (Figure 2f).

### 3.4 | Recording of the nociceptive responses of SpVc neurons

Single neuron unit recording was performed to identify the mechanically stimulated neurons in the SpVc. In sham rats ( $n = 6$ ), a total of 56 neurons were recorded; 22 neurons (38.7%) showed excitatory responses to orofacial nociceptive stimuli, beginning at 15g stimulation

causing 50% above nociceptive threshold as shown in Figure 3a. The firing rates in response to 15, 26, and 60 g mechanical pressure were gradually increased (Figure 3b). In ION-CCI rats ( $n = 6$ ), a total of 45 neurons were recorded, of which 27 neurons (60.0%) were mechanically excited neurons. The neuronal firing rate increased in response to gradually increased orofacial mechanical pressures, but these responses were significantly greater when compared with those of sham rats (Figure 3b;  $F_{2,66(\text{time})} = 150.7$ ,  $F_{1,66(\text{surgery})} = 168.9$ , \* $p < 0.05$ , \*\*\* $p < 0.001$ , two-way ANOVA post hoc Bonferroni test). This is the electrophysiological correlate of allodynia.

### 3.5 | Enhancement of synaptic transmission at the TG-SpVc synapses in ION-CCI rats

In both sham ( $n = 5$ ) and ION-CCI rats ( $n = 5$ ), various electrical stimuli (200–1,000  $\mu\text{A}$ ) in the TG produced gradually increasing SpVc FP amplitudes as shown in Figure 3c. The ION-CCI rats showed markedly enhanced LFP responses evoked by TG stimulations compared with the sham rats (Figure 3c). A clear increase in responsiveness at

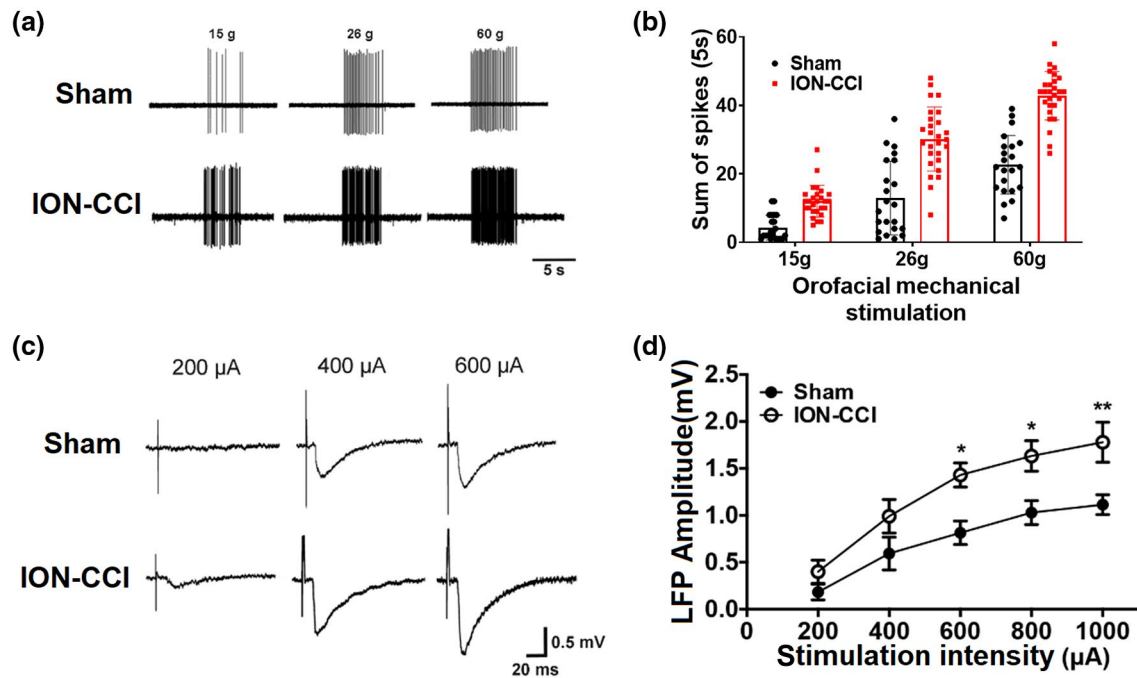


**FIGURE 3** Single unit recording and local field potential recording in the SpVc of ION-CCI and sham rats. (a) Representative recordings of SpVc mechanical excited neurons in response to graded mechanical pressures (15, 26, and 60 g) in sham and ION-CCI rats. (b) The SpVc neuronal firing rates in response to graded mechanical stimuli were markedly increased in ION-CCI rats (two-tailed unpaired *t*-test,  $^{**}p < 0.01$ ,  $^{***}p < 0.001$ ,  $n = 6$  rats in each group,  $N = 56$  neurons in sham and 45 neurons in ION-CCI rats were recorded). (c) Representative curves of LFP responses in the SpVc to different TG stimuli (200, 400, and 600  $\mu$ A) in sham and ION-CCI rats. (d) Left shift of input-output curve in the SpVc of ION-CCI rats ( $n = 5$  in each group). Results are presented as mean  $\pm$  SD. Statistical significance was determined by two-way ANOVA, followed by multiple comparisons adjusted by the Bonferroni's test,  $^{*}p < 0.05$ ,  $^{**}p < 0.01$

all points of the I/O curve above threshold (200 $\mu$ A) was observed in ION-CCI rats, suggesting long-lasting enhancement of TG-SpVc synaptic transmission after constricting the trigeminal nerve (Figure 3d;  $F_{1,40(\text{surgery})} = 23.21$ ,  $^{*}p < 0.05$ ,  $^{**}p < 0.01$ ,  $^{***}p < 0.001$ , two-way ANOVA post hoc Bonferroni test).

To study whether NMDA and AMPA receptors play a role in mediating TG-SpV basal synaptic transmission, we infused NMDA and AMPA receptor antagonist using reverse microdialysis and recorded the signals. The representative recordings of LFP amplitudes after application of CNQX or AP5 in sham and ION-CCI rats are shown in Figure 4a,d. In sham rats ( $n = 5$ ), administration of CNQX (an AMPA receptor antagonist) (1.0 mM,  $n = 5$ ) into the SpVc significantly reduced the basal LFP amplitudes in response to TG stimulations (Figure 4b;  $F_{1,40(\text{surgery})} = 41.39$ ,  $^{***}p < 0.001$ , two-way ANOVA). In contrast, reverse microdialysis of AP5 (NMDA receptor antagonist) (2.0 mM,  $n = 5$ ) did not reduce the LFP amplitudes (Figure 4e;  $F_{1,40(\text{surgery})} = 0.27$ , n.s.,  $p > 0.05$ , two-way ANOVA). These results signify that AMPA receptors play a major role in mediating TG-SpVc basal synaptic transmission.

In ION-CCI rats ( $n = 10$ ), administration of CNQX ( $n = 5$ ) also reduced the TG-SpVc amplitudes in response to TG stimulation (Figure 4c;  $F_{1,40(\text{surgery})} = 58.00$ ,  $^{***}p < 0.001$ , two-way ANOVA). In contrast to sham control rats, reverse microdialysis of AP5 ( $n = 5$ ) did reduce the LFP amplitudes (Figure 4f;  $F_{1,40(\text{surgery})} = 37.77$ ,  $^{***}p < 0.001$ , two-way ANOVA). These results suggest that both

AMPA receptor and NMDA receptors contribute to the enhanced TG-SpVc basal synaptic transmission in ION-CCI rats determined by two-way ANOVA, followed by multiple comparisons adjusted by the Bonferroni's test.

### 3.6 | Recording of the nociceptive responses of ACC neurons in ION-CCI rats

To clarify whether neurons in the ACC region were involved in mediating hypersensitivity in ION-CCI rats, neural activity in the ACC is recorded while applying mechanical stimulation in the face in anaesthetized rats. In the sham rats ( $n = 5$ ), a total of 52 ACC neurons were recorded. The sample recordings of ACC neuronal responses to graded orofacial mechanical stimuli in anaesthetized rats are shown in Figure 5a. The firing rates gradually increased in response to mechanical pressure (Figure 5b;  $F_{2,255(\text{stimulation})} = 80.12$ ,  $^{***}p < 0.001$ , two-way ANOVA). In ION-CCI rats ( $n = 5$  rats), a total of 48 neurons were recorded. The neuronal firing rates of these neurons in ION-CCI rats also significantly increased in response to gradually increased orofacial mechanical pressures, and the activity at all levels of nociceptive stimulation was increased by at least 50% compared with those of sham rats (Figure 5b;  $F_{1,255(\text{surgery})} = 92.78$ ,  $^{***}p < 0.001$  two-way ANOVA). Power spectral analysis was performed during 120 s in home cage in awake resting state in sham-operated and

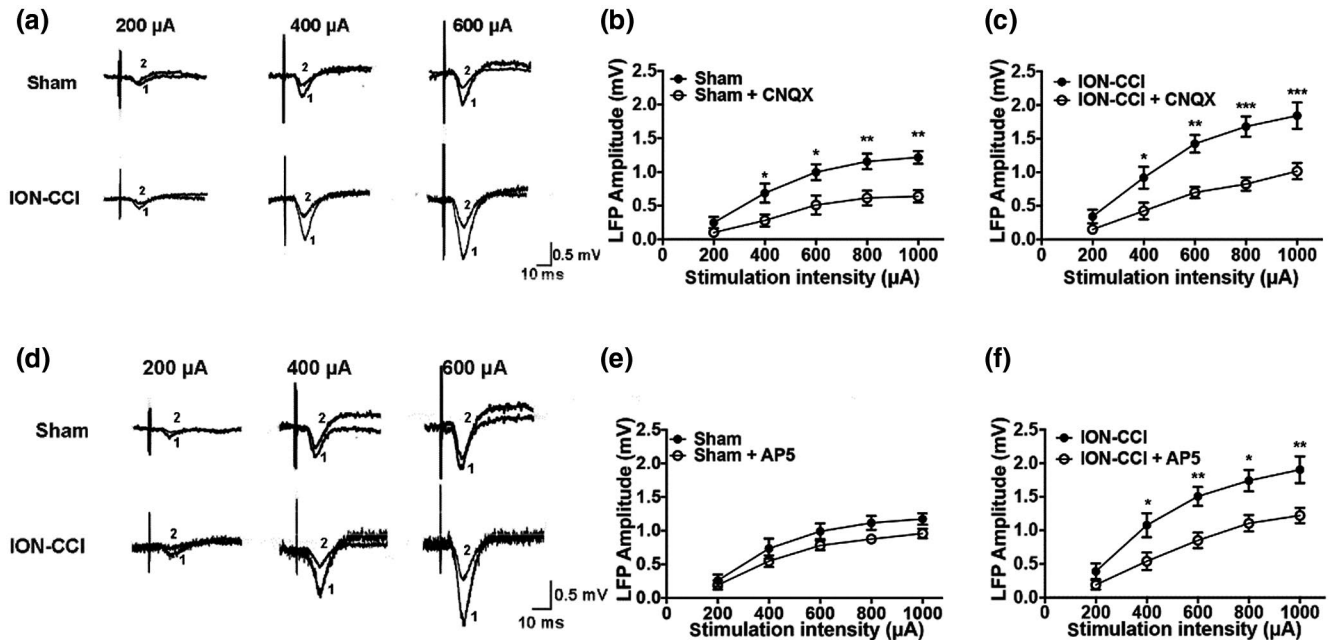


**FIGURE 4** Effect of glutamatergic receptor antagonists on SpVc-LFP in ION-CCI and sham rats. (a) Representative curves of LFP responses in the SpVc to different TG stimuli (200, 400, and 600  $\mu\text{A}$ ) after reverse microdialysis of vehicle (ACSF, 1) and AMPA receptor antagonist CNQX (1.0 mM, 2) in sham and ION-CCI rats on Day 8 postsurgery. (b) In sham rats, input-output curve (I-O) was significantly decreased after CNQX (\* $p < 0.05$ , \*\* $p < 0.01$ ,  $n = 5$ ) administration compared with the vehicle. (c) In ION-CCI rats, I-O curve was significantly decreased after CNQX (\* $p < 0.05$ , \*\* $p < 0.01$  and \*\*\* $p < 0.001$ ,  $n = 5$ ) administration compared with vehicle. (d) Representative curves of LFP responses in the SpVc to different TG stimuli (200, 400, and 600  $\mu\text{A}$ ) after reverse microdialysis of vehicle (ACSF, 1) and NMDA receptor antagonist AP5 (2.0 mM, 2) in sham and ION-CCI rats on Day 8 postsurgery. (e) In sham rats, input-output curve was not changed significantly after AP5 ( $n.s p > 0.05$ ,  $n = 5$ ) administration compared with the vehicle. (f) In ION-CCI rats, I-O curve was significantly decreased after AP5 administration compared with vehicle (\* $p < 0.05$ , \*\* $p < 0.01$ ,  $n = 5$ ). Results are presented as mean  $\pm$  SD. Statistical significance for figure b, d, and f was determined by two-way ANOVA, followed by multiple comparisons adjusted by the Bonferroni's test

ION-CCI rats. There was no significant difference in the power spectral density and different oscillation band in the ACC region between the two groups (Figure 5c-f,  $t_{13} = 0.7173$   $p = 0.486$  for delta band;  $t_{13} = 0.0759$   $p = 0.94$  for theta band;  $t_{13} = 0.0356$   $p = 0.972$  for beta band).

### 3.7 | Impaired ACC-BLA spike-field phase synchrony during the late stages of chronic neuropathic pain

To identify the changes taking place after ION-CCI in cortical regions of awake rats, the single unit recordings from the ACC and the LFP in the BLA region were compared, and the SFC values between the ACC spikes and the BLA LFP were computed. ION-CCI rats ( $n = 7$ ) displayed a decrease in SFC in the low-frequency range compared to sham rats ( $n = 8$ ) (Figure 6a;  $n = 52$  neurons for control group,  $n = 48$  neurons for ION-CCI group,  $F_{1, 1188(\text{surgery})} = 11.86$ , \*\*\* $p < 0.001$ , two-way ANOVA). The averaged SFC values in theta range (4–10 Hz) were significantly decreased from  $6.075\% \pm 2.541\%$  to  $3.228\% \pm 1.489\%$  in the ION-CCI rats (Figure 6b;  $t_{98} = 6.763$ , \*\*\* $p < .001$ , two-tailed unpaired  $t$ -test). In addition to that, the percentage of phase-locked neurons in the theta band decreased from  $29.375\% \pm 6.203\%$

in sham rats to  $10.85\% \pm 4.032\%$  in the ION-CCI rats (Figure 6c,d,  $t_{13} = 2.422$ ,  $p = 0.031$ , unpaired  $t$ -test).

We also computed the cross-correlation between the LFP-filtered data from ACC and BLA. The ratio of second peak to that of positive peak of the cross-correlation coefficient notably decreased in ION-CCI rats (Figure 7a,b;  $t_{13} = 2.208$ ,  $p = 0.047$ , two-tailed unpaired  $t$ -test). Previous references indicate that the ratio of second peak to the positive peak of the cross-correlation coefficient was positively related to the good decision-making in rats. These results suggest that reduced BLA to ACC information flow might contribute to undecided and poor decision-making performance. Among the sham rats, four of them showed high cross-correlation between ACC and BLA and three of them showed low cross-correlation values (Figure 7c) and all the ION-CCI rats showed low cross-correlation values (Figure 7c). BLA-ACC lag estimates showed that the cross-correlation peak was located at negative lags among ION-CCI and sham rats (Figure 7d), signifying an information flow directionality from the BLA to the ACC. Sham group rats depicted a consistent information flow from the BLA to the ACC (mean lag =  $-16.00 \pm 16.82$ ;  $n = 7$  sham rats), whereas the information flow is disrupted in the ION-CCI (Figure 7e; mean lag =  $-49.715 \pm 25.56$ ;  $n = 8$  ION-CCI rats,  $p = 0.009$  two-tailed unpaired  $t$ -test).



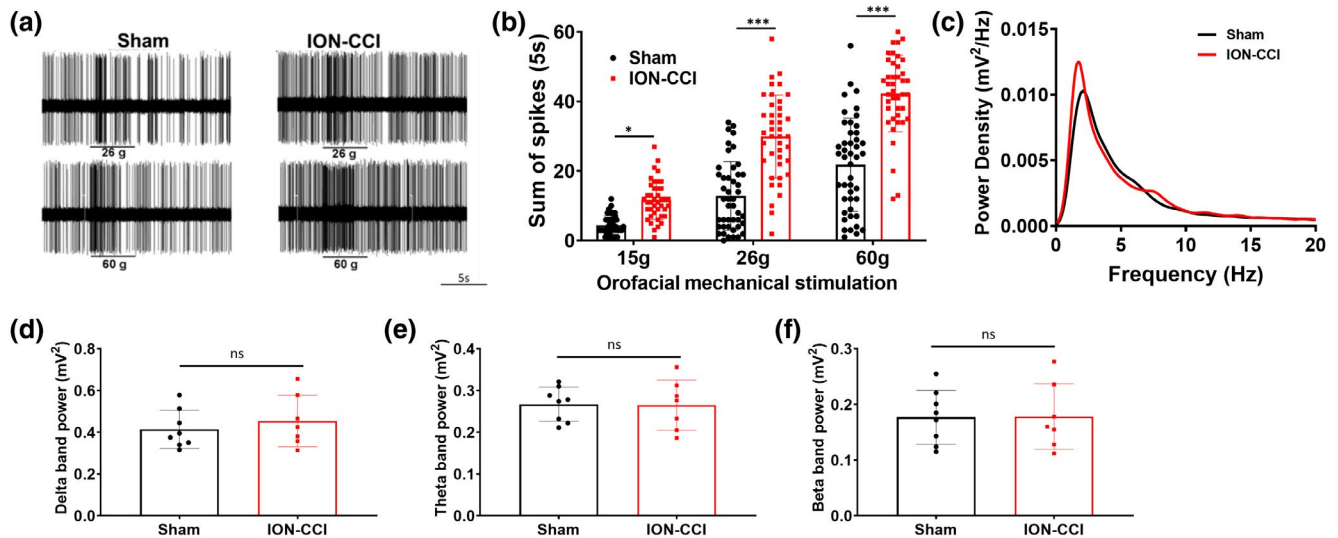


**FIGURE 5** Recording of ACC neuron firing rate and power spectral density in ION-CCI rats and sham rats. (a) Representative recordings of ACC mechanical excited neurons in response to graded pressures in sham and ION-CCI rats. (b) ACC spike firing rates in response to graded mechanical stimuli were markedly increased in ION-CCI rats ( $N = 48$  neurons) compared to sham-operated rats ( $N = 52$  neurons),  $n = 5$  rats per group  $*p < 0.05$ ,  $***p < 0.001$ , two way unpaired Student  $t$ -test. (c) Power spectral density analysis in the frequency range from 0 to 20 Hz of the LFP in the ACC in 30-day ION-CCI and sham-operated rats ( $n.s.$ ,  $p > 0.05$ , two way unpaired Student  $t$ -test). (d) Histograms showing the averaged delta band power (0.5–4 Hz), theta band power (4–10 Hz), and beta band power (10–20 Hz) in the ACC region in 30-day ION-CCI and sham-operated rats ( $n.s.$ ,  $p > 0.05$ )

### 3.8 | Trigeminal neuropathy causes ACC hypomyelination

Pain originates in the central or peripheral nervous system frequently becomes centralized through maladaptive responses within the central nervous system that can profoundly alter brain systems and thereby behavior. White matter integrity is disturbed in chronic pain states. To identify the effect of chronic neuropathy on mPFC myelination, rats were sacrificed 30 days after the ION-CCI surgery and ACC tissue sections were collected. The schematic representation of the location of ACC region is shown in Figure 8a. MBP, a biomarker for myelin basic protein was examined using Western blotting and immunofluorescent microscopy. Western blot analysis, performed after normalizing to sham controls, revealed lower MBP expression in ION-CCI rats compared to sham rats (Figure 8b,c; ION-CCI =  $0.710 \pm 0.32$ ; sham =  $1.00 \pm 0.120$ ;  $t_6 = 3.231$ ;  $p = 0.0179$ ;  $n = 4$  rats per group, unpaired  $t$ -test; unprocessed Western blot in Figure S1). Immunostaining images showed lower expression of MBP in the ACC of the ION-CCI group compared to that of sham-operated controls (Figure 8d). Quantitative analysis showed a lower intensity of MBP+ fibers in the ION-CCI rats compared to the sham-operated controls (Figure 8f; ION-CCI =  $0.772 \pm 0.167$ ; sham =  $1.000 \pm 0.170$ ;  $t_{10} = 2.343$ ;  $p = 0.0411$ ;  $n = 6$  rats per group, unpaired  $t$ -test). We further studied the microstructure using TEM analysis and showed that the myelin sheath thickness was reduced in ION-CCI rats (Figure 8e). The quantitative assessment of the G-ratio of myelinated fibers revealed lower thickness of myelin sheath in ION-CCI rats than the sham control (Figure 8 G,H; ION-CCI =  $0.71 \pm 0.052$ ; sham =  $0.611 \pm 0.0564$ ;  $t_{238} = 14.35$ ;  $p < .0001$   $n = 120$  axons per

group, unpaired  $t$ -test), whereas the thickness of axons had not been altered (Figure 8i; ION-CCI =  $1.076 \pm 0.454$ ; sham =  $1.038 \pm 0.424$ ;  $t_{238} = 1.143$ ;  $p = 0.4674$ ,  $n = 120$  axons, unpaired  $t$ -test).

### 3.9 | Chronic neuropathic pain decreases oligodendrocyte progenitor cells and mature oligodendrocytes in the ACC

Oligodendrocyte progenitor cells (OPCs) are subtype of glial cells that are mitotically active and uniformly distributed throughout the brain. OPCs are characterized only by their expression of a specific antigen—the proteoglycan NG2. NG2-glia can differentiate into OLs and are also responsible for the self-renewal of OPCs under physiological conditions. Anti-adenomatous polyposis coli clone CC1 (abbreviated as CC1) antibody is the most used to specifically label mature OLs without labeling myelin. To characterize the effect of chronic TNP on OPC proliferation and OL genesis, we performed immunohistochemistry to determine the absolute number of OPCs (NG2+ cells,) and OLs (CC1+ cells,) in the ACC of ION-CCI and control rats. We observed that the number of NG2+ OPCs were decreased to 51.98% in ION-CCI rats compare to control (Figure 9a,b;  $561.6 \pm 133.4$  cells/mm<sup>2</sup> for ION-CCI versus  $965.0 \pm 202.3$  cells/mm<sup>2</sup> for sham;  $t_{10} = 4.077$ ;  $p = 0.0022$ ;  $n = 6$  rats per group, unpaired  $t$ -test). We further observed that  $28.73\% \pm 8.25\%$  NG2+ cells were colabeled with Olig2 in ION-CCI rats which was  $16.47\%$  lower than that of the sham ( $45.2\% \pm 9.31\%$ ) indicating, a reduction in number of reactive OPCs that were ready for differentiation (Figure 9c;  $t_{10} = 3.251$ ;  $p = 0.0087$ ;  $n = 6$  rats per group, unpaired



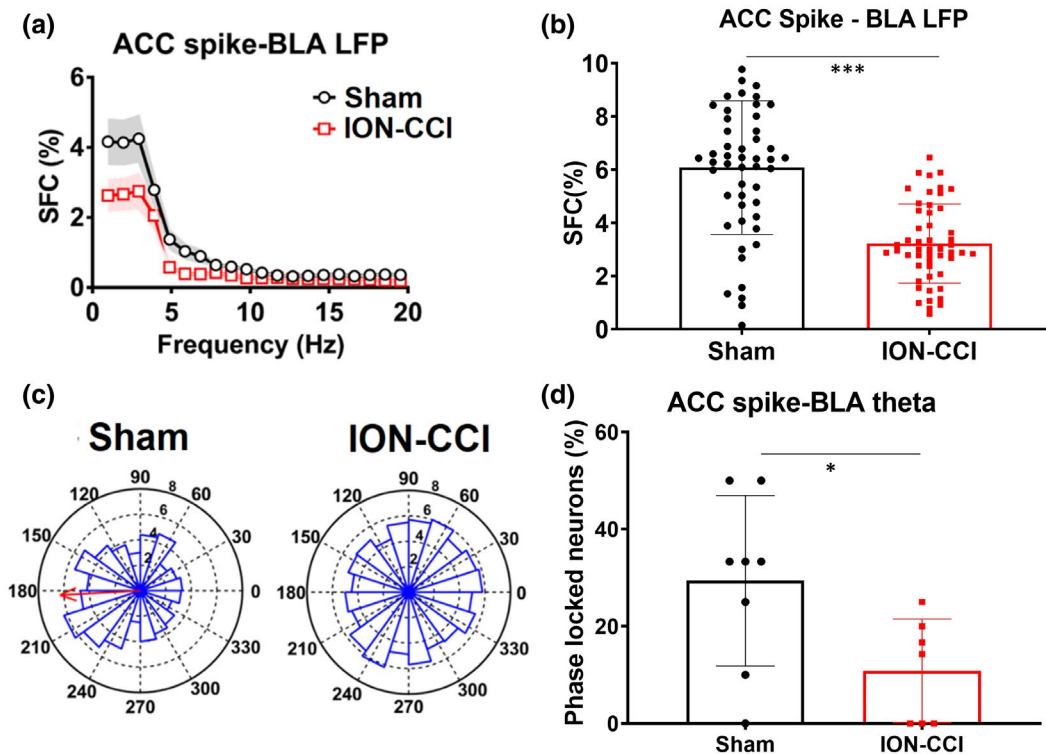


**FIGURE 6** Reduction of spike-field coherence and phase locking between ACC spikes and BLA theta in ION-CCI rats. (a) The SFC distribution of ACC single units as a function of frequencies in sham ( $n_{\text{rats}} = 8$ ,  $n_{\text{neurons}} = 52$ ) and ION-CCI rats ( $n_{\text{rats}} = 7$ ,  $n_{\text{neurons}} = 48$ ). Shadow areas represent SD. (b) Averaged SFC values in theta band show reduction of theta band SFC in ION-CCI rats compared to that in the sham rats ( $n = 52$  neurons for sham and 48 neurons for ION-CCI,  $***p < 0.001$ , two-tailed unpaired  $t$ -test). (c) Examples show polar histograms of the ACC spike timing-BLA theta phase distribution of single unit recorded in the ACC in one sham and ION-CCI rat. The red arrow in the polar histogram of sham rat represents angle of the mean resultant vector. (d) Averaged percentages of phase-locked neurons show a significantly decrease in ACC single-unit spikes phase locking to BLA theta band field potential in ION-CCI rats. Results are shown as mean  $\pm$  SD ( $*p < 0.05$ , two-tailed unpaired  $t$ -test)

$t$ -test). Anti-adenomatous polyposis coli clone CC1 (abbreviated as CC1) antibody is the most used to specifically label mature OLs without labeling myelin. In this study, we used CC1 to mark the mature OLs and observed a significant decrease in the absolute number of CC1+ OLs in ION-CCI rats than sham controls (Figure 9d,e;  $175.3 \pm 35.2$  cells/mm<sup>2</sup> for ION-CCI versus  $284.8 \pm 66.9$  cells/mm<sup>2</sup> for sham;  $t_8 = 3.555$ ;  $p = 0.0052$ ;  $n = 6$  rats per group, unpaired  $t$ -test). We further observed that 19.7% CC1+ cells were colabeled with Olig2 in ION-CCI rats which was 21.1% lower than the control (Figure 9f;  $19.7\% \pm 7.73\%$  cells for ION-CCI versus  $40.8\% \pm 6.24\%$  cells for sham;  $t_{10} = 5.20$ ;  $p = 0.0004$ ).

### 3.10 | Neuropathic pain correlates with microglial activation and pro-inflammatory cytokines expression

Neuroinflammation is a pro-inflammatory cytokine-mediated process that is associated with nerve tissue injury. Therefore, we are curious to see whether neuroinflammation cells are also reactive in our ION-CCI rat model. To characterize this, we performed Western blotting and immunohistochemistry to determine the relative expression of pro-inflammatory cytokines (IL-1 $\beta$  and CD68)

and IBA1+ cells (biomarker for reactive microglia) in the ACC of ION-CCI and sham rats. Western blot studies revealed that CD68 expression was increased in ION-CCI rats compared to sham rats (Figure 10a,b;  $1.306 \pm 0.141$  for ION-CCI versus  $1.00 \pm 0.083$  for sham;  $t_5 = 3.296$ ;  $p = 0.021$ ;  $n = 3$  sham rats and  $n = 4$  ION-CCI rats, unpaired  $t$ -test; unprocessed Western blot in Figure S2). Also, IL-1 $\beta$  protein expression was increased in ION-CCI rats compared to sham rats (Figure 10a,c;  $1.64 \pm 0.062$  for ION-CCI versus  $1.00 \pm 0.081$  for sham;  $t_5 = 11.92$ ;  $p < 0.001$ ;  $n = 3$  sham rats and  $n = 4$  ION-CCI rats, unpaired  $t$ -test). Immunofluorescence studies showed increased activation of IBA1+ microglia as observed by increased fluorescence in the ACC of ION-CCI rats after normalizing with that of control rats (Figure 10d,e,  $1.815 \pm 0.419$  for ION-CCI versus  $1.00 \pm 0.185$  for sham;  $t_8 = 3.296$ ;  $p = 0.0041$ ;  $n = 5$  rats per group, unpaired  $t$ -test). Also, there was increased colabeling of CD68 with IBA1+ microglia indicating pro-inflammatory cytokines released from activated microglia. The number of colabeled IBA1+ CD68+ microglial cells increased to  $51.72 \pm 17.37$  microglia/mm<sup>2</sup> in ION-CCI rats compared to  $23.51 \pm 8.23$  microglia/mm<sup>2</sup> in sham rats (Figure 10f,  $t_8 = 3.283$ ,  $p = 0.011$ ;  $n = 5$  rats per group, unpaired  $t$ -test). Similarly, higher expression of pro-inflammatory cytokines marker IL-1 $\beta$  was observed in ION-CCI rats (Figure 10g,h,  $1.353 \pm 0.284$  for ION-CCI versus

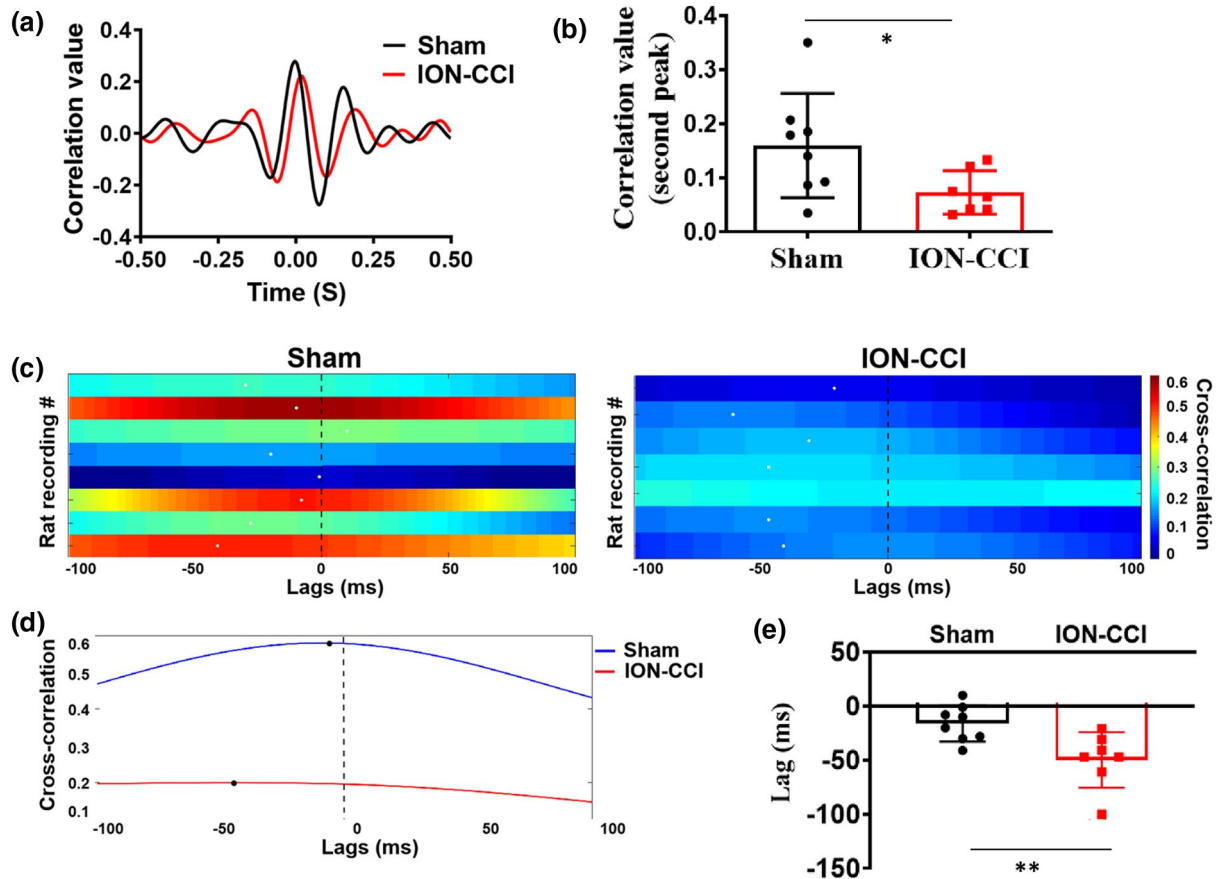


**FIGURE 7** Disrupted BLA-ACC LFP theta coherence and information flow in ION-CCI rats. (a) Cross-correlation analysis of theta-filtered LFP recorded in the BLA and ACC revealed a reduction of synchronization in theta band in ION-CCI rats compared to sham rats ( $***p < 0.001$ ). (b) Averaged cross-correlation value of second positive peak which represents synchronization of theta band LFP between the BLA and the ACC showed the synchronization was decreased in ION-CCI rats ( $*p < 0.05$ , two-tailed unpaired *t*-test). (c) Lag estimate for sham ( $n = 8$ ), ION-CCI rats ( $n = 7$ ) by cross-correlation amplitude of field potential recorded from BLA and ACC. Warmer colors indicate higher cross-correlation peaks or greater phase-locking strength. White dots represent the lags at which the cross-correlation coefficient peaks occurred. (d) Representative distributions of cross-correlation coefficient at different lags from examples of one sham rat (blue line) and ION-CCI rat (red line). Dark stars show the peaks of the cross-correlation. (e) The reduction of mean lags at the peak in ION-CCI rats were compared to sham rats.  $**p < 0.01$  by unpaired *t*-test

$1.00 \pm 0.128$  for sham;  $t_8 = 2.507$ ;  $p = 0.037$ ;  $n = 5$  rats per group, unpaired *t*-test) compared to sham rats indicating neuroinflammation in response to chronic neuropathic pain.

## 4 | DISCUSSION

The definition of chronic pain remains tautological, because it simply asserts that it is a long-lasting pain, or a pain persisting past the normal healing period. Patients with TNP who approach dentists with severe and persistent pain do not exhibit clinical or radiographic abnormalities and are unresponsive to treatment with analgesics or surgery. The mechanisms underlying the transition from acute to chronic pain, such as prolonged “pain memory” known as “atypical odontalgia” (Talbot et al., 1991) and “phantom tooth pain” (Marbach, 1993), remain unclear. The ION-CCI has become the most popular TNP injury animal model due to the robust induction of chronic allodynia and hyperalgesia (Kim & Nabekura, 2011). The

orofacial afferent nociceptive inputs which enhance synaptic transmission leading to a reduction in the pain threshold are well recognized (Sessle, 2005). The spinal-brainstem-spinal positive feedback loop has been proposed to be involved in the maintenance of neuropathic pain states (Deng, 2010). However, pharmacological and surgical manipulation of this loop produced short- (Willloch et al., 2003), instead of long-term relief from allodynia, shifting the consideration to other supraspinal areas (Apkarian et al., 2009; Sessle, 2005). Ascending multisynaptic pathways from the TG through the SpV and medial thalamus (MT) to the ACC have been identified (Iwata et al., 2011). Neuropathic pain can spur changes in LFPs in multiple frequency bands in ACC (Li et al., 2017). Human brain-imaging studies (Borsook et al., 2003; Witting et al., 2006) have shown enhanced activation in these areas in response to stimuli of the trigger zone in patients with TNP. Here, we used the ION-CCI model to create stable allodynia lasting at least 5 weeks (Figure 1). Electrophysiological recordings demonstrated that the SpVc neuronal firing rate increased in response to gradually increased orofacial mechanical

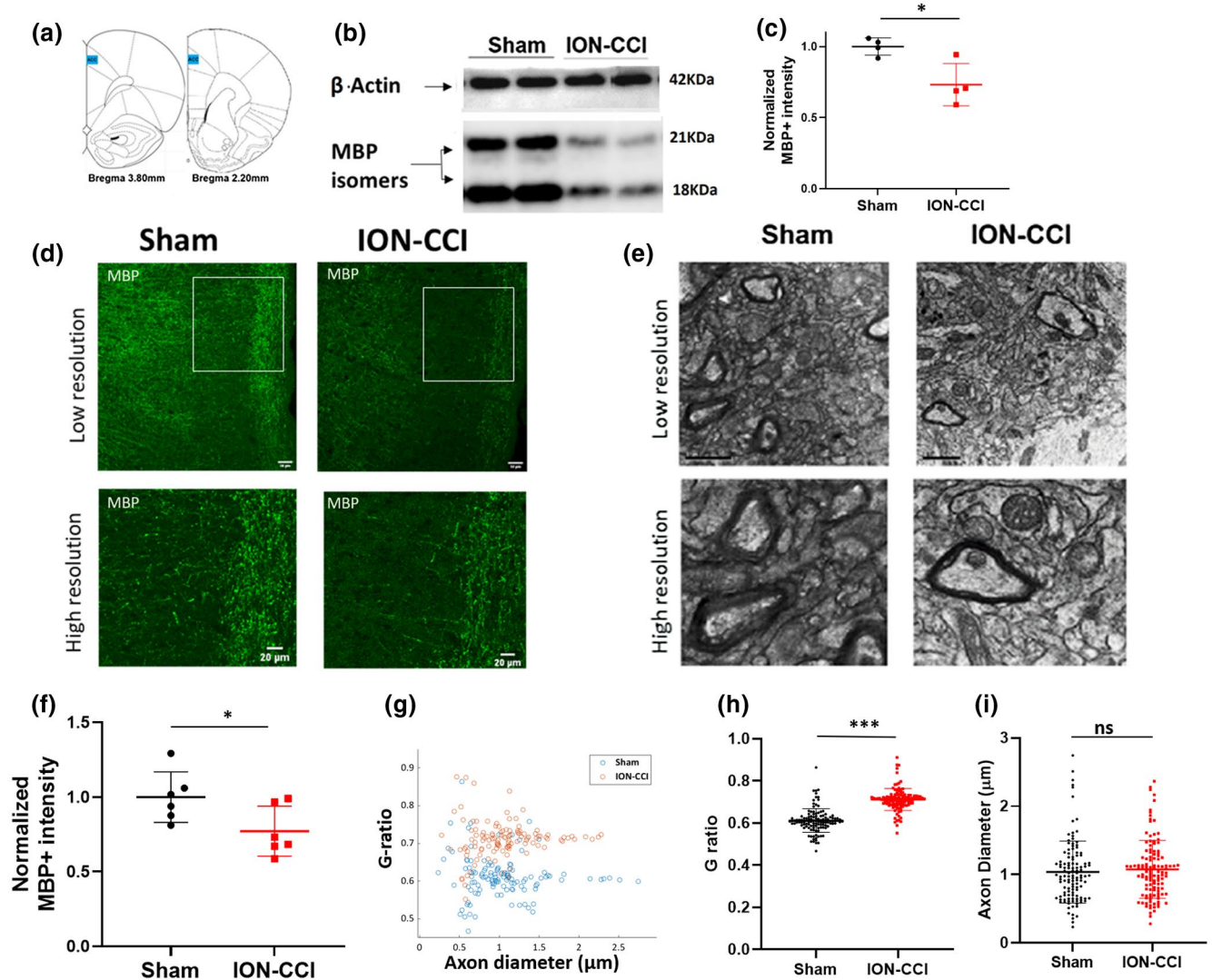


**FIGURE 8** Myelin expression is decreased in the right ACC region of ION-CCI rats. (a) Schematic representation of the ACC region (blue squares) immunostained sections from 3.8 to 2.2 mm from the bregma. Also ACC regions are targeted for Western blot analysis. (b) Representative Western blot images of MBP and  $\beta$ -actin in the ACC extracts from sham and ION-CCI rats using anti-MBP antibody. (c) The Western blot images in Figure 8b are quantified and mean MBP intensity in ION-CCI rats were found to be lower compared to that of sham rats. Data are shown as mean  $\pm$  SD ( $n = 4$  sham rats;  $n = 4$  ION-CCI rats).  $*p < 0.05$ , unpaired Student's *t*-test. (d) Representative confocal images of MBP in the ACC region show decreased expression of myelin basic protein in ION-CCI rats compared to sham-operated rats. Scale bar: 20  $\mu$ m. (e) Electron micrographs (EM) of ACC region showing myelinated axons in ION-CCI and sham rats ( $n = 3$  rats per group). Scale bar: 200 nm. (f) Relative intensity of MBP fluorescent in the ACC, sections from 2.2 to 3.8 mm from the bregma for the figure (d). The MBP mean fluorescent intensity was decreased in ION-CCI rats (mean  $\pm$  SD;  $n = 6$  rats in each group;  $*p < 0.05$ ; unpaired Student's *t*-test). (g) Scatterplot of G-ratios in sham rats (blue circle,  $n = 3$  rats) and ION-CCI rats (red circle,  $n = 3$  rats). (h) Average G-ratio of myelinated axons in the ACC region in ION-CCI and sham rats. Data are shown as mean  $\pm$  SD ( $n = 120$  axons from 3 rats per group).  $***p < 0.001$ , unpaired student's *t* test. (i) Axonal diameters do not change significantly among group. Data are shown as mean  $\pm$  SD ( $n = 120$  axons from 3 rats per group).  $p > 0.05$ , unpaired Student's *t*-test

pressures, but these responses were significantly greater in the TNP rats when compared with those of sham rats. Further, the ION-CCI rats showed markedly a long-lasting enhancement of the LFP in the TG-SpVc synapses, and this enhancement was reduced by the blockade of NMDA receptors (Figures 3 and 4). This long-lasting LFP enhancement at the first synapse from the TG to the SpV can play a role in the development of hyperalgesia.

The ACC encompasses various cognitive functions, including sensory perception, attention, memory, emotional and

motivational responses (Hasan et al., 2019; Hutchison et al., 1999; Talbot et al., 1991; Vogt et al., 1993; Wang et al., 2017). Chronic pain is reduced in patients with ACC lesions (Davis et al., 1994).

There is an increased neuronal excitability (Li et al., 2010) and evidence for synaptic potentiation in the ACC in acute and chronic pain (Bliss et al., 2016). In the case of chronic visceral pain, our previous work has characterized the electrophysiological activity of the ACC during processing of visceral nociceptive stimulation. Our previous studies have identified the enhanced neuronal responses in the ACC



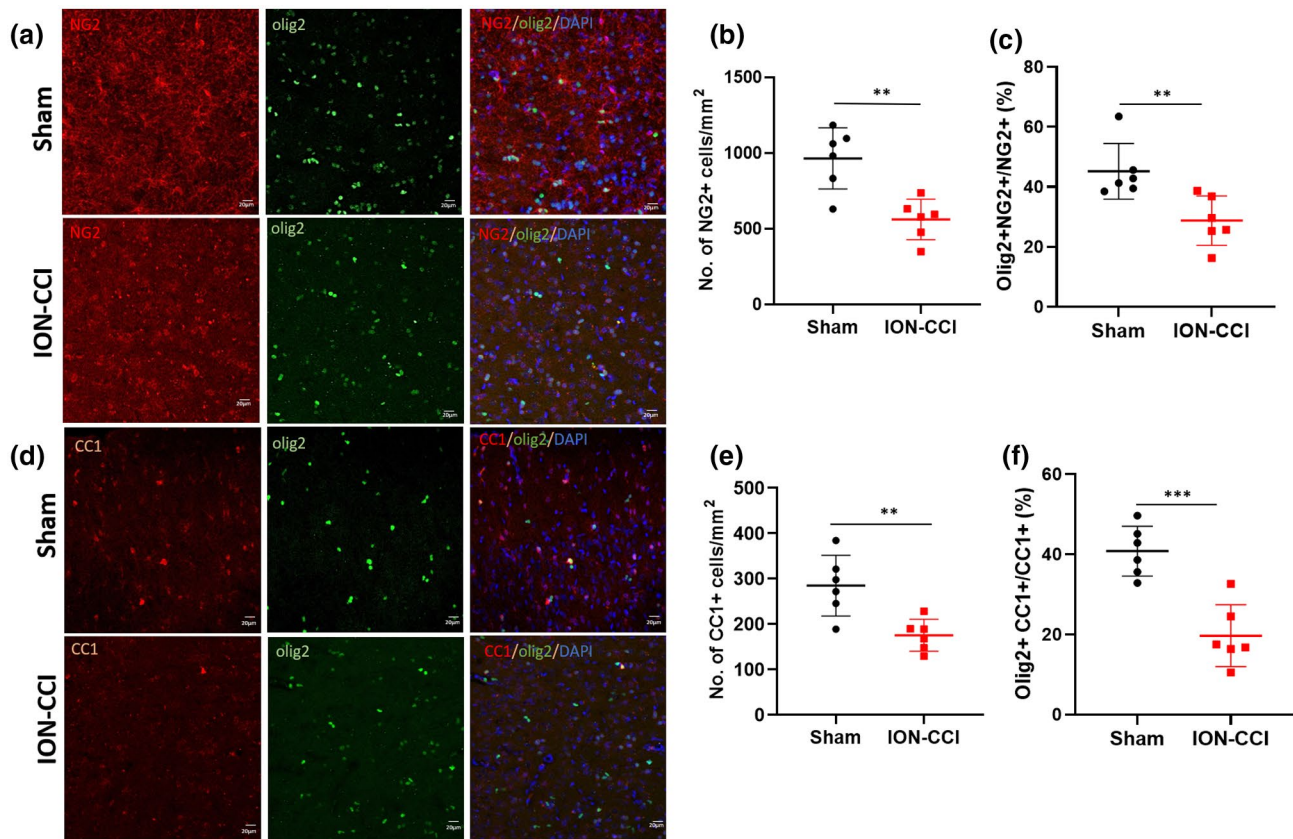


**FIGURE 9** Neuropathic pain impairs oligodendrocyte progenitor cell proliferation and oligodendrocyte production in ION-CCI rats. (a) Representative confocal micrograph of Olig2+ (green, a biomarker for oligodendrocyte transcription factor) colabeled with NG2+ (red) OPCs in the ACC of ION-CCI and sham rats. Scale bars: 20  $\mu$ m. (b) Total number of NG2+ cells in the ACC of ION-CCI and sham rats. Data are shown as mean  $\pm$  SD ( $n = 6$  rats per group). \*\* $p < 0.01$ , unpaired Student's  $t$ -test. (c) Total percentage of Olig2+ NG2+ OPC in the ACC of ION-CCI and sham rats. Data are shown as mean  $\pm$  SD ( $n = 6$  rats per group). \*\* $p < 0.01$ , unpaired Student's  $t$ -test. (d) Representative confocal images of CC1+ (red), colabeled with Olig2+ (green) indicating mature OLs in the ACC of ION-CCI and sham rats. Scale bar: 20  $\mu$ m. (e) Total number of CC1+ oligodendrocyte (OL) cells in the ACC of ION-CCI and sham rats. Data are shown as mean  $\pm$  SD ( $n = 6$  rats per group). \*\* $p < 0.01$ , unpaired Student's  $t$ -test. (f) Total percentage of Olig2+ CC1+ mature OLs cells in the ACC of ION-CCI and sham rats. Data are shown as mean  $\pm$  SD ( $n = 6$  rats per group). \*\*\* $p < 0.001$ , unpaired Student's  $t$ -test

to visceral stimulation in VH rats (Gao et al., 2006). The activation of ACC is critical for pain sensitivity (Cao et al., 2008; Fan et al., 2009) and long-term visceral affective memory (Yan et al., 2012). We and other investigators have showed that LTP can no longer be induced by theta-burst stimulation in rodent model of VH (Wang et al., 2015) and neuropathic pain (Bliss et al., 2016; Li et al., 2010), indicating that maximal potentiation has already occurred. In this study, we performed electrophysiological recording to show enhanced ACC mechanical excited neurons in response to graded pressures in ION-CCI rats suggesting ACC sensitization in rats with chronic TNP. However, as observed in VH rats (Gao et al., 2006), neuronal responses evoked by colorectal distention did not exhibit significant change, indicating that a collection of ACC neurons is capable of discriminative coding for hypersensitivity, specifically for ION-CCI.

Hossaini et al. (2010) showed that Arc protein was increased in neuropathic rats in the early phase in spinal cord. There is a persistent activation of afferent fibers in chronic neuropathic pain and increase of c-Fos expression in the orbitofrontal cortex (Leite-Almeida

et al., 2014). In this study, we confirm that there is an elevation of c-Fos proteins in the ACC in the chronic neuropathic pain rats after mechanical stimulation (Figure 1c,d), indicating ION-CCI-induced chronic neuropathy causes plasticity in the ACC.

Studies in humans and animals have suggested that chronic pain impedes neuropsychological function (Hart et al., 2000). Although it has been suggested that there are common "signature" changes in chronic pain in the cingulate cortex, the orbitofrontal cortex, and the insula (Hu, 2016; May, 2008; Zhuo, 2019), there has been no animal model established to study pain-related cognitive deficits and its underlying mechanisms.

Decision-making under complex and uncertain circumstances is a fundamental cognitive process that requires adaption relying on the integration of several executive functions. Impaired decision-making has been demonstrated to represent a key symptom in many mental disorders (Paulus, 2007; Rahman et al., 2001). In humans, decision-making has been accurately modeled using the Iowa gambling task (IGT) in the laboratory (Bechara et al., 1997, 2000). In this study, we

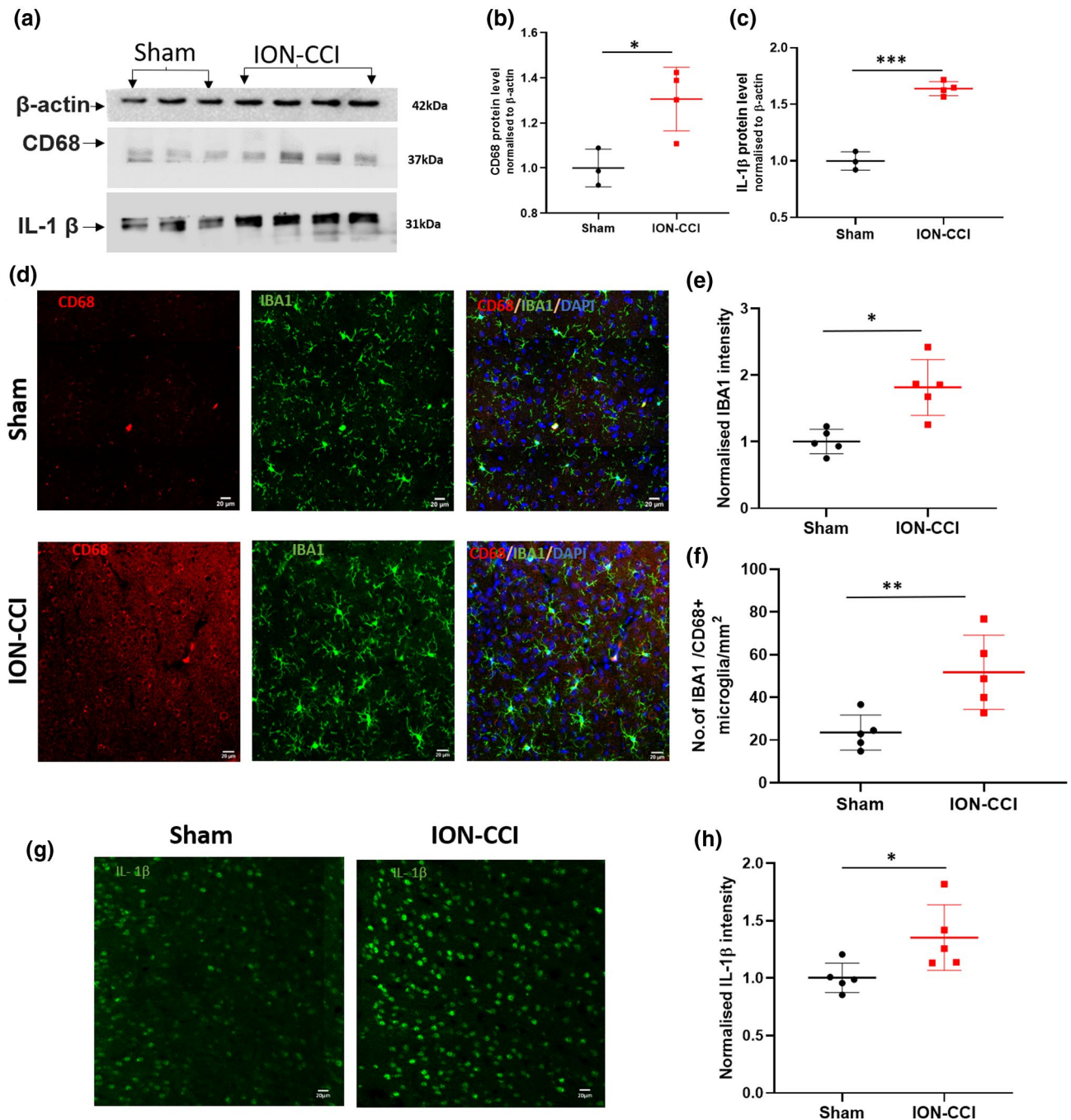


**FIGURE 10** Increased microglial activity and cytokine expression in ION-CCI rats. (a) Western blot images of CD68, IL-1 $\beta$ , and  $\beta$ -actin in the ACC extracts from sham and ION-CCI rats using anti-MBP antibody. (b) The CD68 Western blot images in Figure 10a are quantified and normalized with  $\beta$ -actin protein levels. The mean CD68 protein intensity in ION-CCI rats was found to increase compared to that of sham rats. Data are shown as mean  $\pm$  SD ( $n = 3$  sham rats;  $n = 4$  ION-CCI rats). \* $p < 0.05$ , unpaired Student's  $t$ -test. (c) The IL-1 $\beta$  Western blot images in Figure 10a are quantified and normalized with  $\beta$ -actin protein levels. The mean IL-1 $\beta$  protein intensity in ION-CCI rats was found to increase than that of sham rats. Data are shown as mean  $\pm$  SD ( $n = 3$  sham rats;  $n = 4$  ION-CCI rats). \*\*\* $p < 0.001$ , unpaired Student's  $t$ -test. (d) Representative confocal micrograph of IBA1 (green) colabeled with CD68+ (red) microglial cells in the ACC of sham and ION-CCI rats. Scale bars: 20  $\mu$ m. (e) The fluorescence intensity of IBA1-stained sections in the ACC of ION-CCI was assessed and normalized to sham rat data. Data are shown as mean  $\pm$  SD ( $n = 5$  rats per group). \* $p < 0.05$ , unpaired Student's  $t$ -test. (f) Total number of CD68+ IBA1+ microglial cells in the ACC of ION-CCI and sham rats are presented. Data are shown as mean  $\pm$  SD ( $n = 5$  rats per group). \*\* $p < 0.01$ , unpaired Student's  $t$ -test. (g) Representative confocal micrograph of IL-1 $\beta$  (green) in the ACC of ION-CCI and sham rats. Scale bars: 20  $\mu$ m. (h) The fluorescence intensity of IL-1 $\beta$ -stained sections in the ACC of ION-CCI was assessed and normalized to sham rat data. Data are shown as mean  $\pm$  SD ( $n = 5$  rats per group). \* $p < 0.05$ , unpaired Student's  $t$ -test



used a RGT (Cao, Wang, Mu, et al., 2016; Cao, Wang, Shahed, et al., 2016; Cao, Wang, Zhang, et al., 2016; Rivalan et al., 2009; Zeeb & Winstanley, 2013) to evaluate cognitive function after chronic ION lesion, and observed significant decreases in the proportion of good decision makers from 77.3% in the control to 45.5% in the chronic ION-CCI rats. We also found marked increases in the numbers of animals that did not learn the task after chronic ION-CCI. These data provide the first evidence that ION lesion impairs decision-making in rats (Figure 2).

The brain is arranged into small- and large-scale levels of organization (Hu et al., 2020; Lu et al., 2016; Varela et al., 2001). Large-scale neural oscillations are fundamental for regulating and redirecting information flow in the brain. Field potential oscillations modulate local spike timing. The tight coordination of spike timing with the local theta frequency band oscillations precedes memory formation in humans (Colgin, 2013; Düzel et al., 2010; Rutishauser et al., 2010), and contributes to the modulation of decision-making behavior in rats (Cao, Wang, Mu, et al., 2016; Cao, Wang, Zhang, et al., 2016; Mu et al., 2015). A plethora of evidence has established that alterations to CNS myelination are involved in learning and memory processes with broad implications for plasticity within adult neural circuitry (McKenzie et al., 2014; Xiao et al., 2016; Xin & Chan, 2020). However, direct *in vivo* evidence of chronic pain-induced myelin disruption and associated OL dysfunction has yet to be reported. Here, our immunohistochemistry and Western blot data demonstrated a reduced expression of MBP in the ACC of TNP rats (Figure 9). NG2 cells are one of the most proliferative glial cell populations in the CNS. In the adult brain, OPCs normally linger in its inactive form. However, demyelination associated with neurological deficit has been observed in several multiple sclerosis and other neurodegenerative diseases. In this study, we observed that total number of OPCs (NG2<sup>+</sup>) were decreased in TNP rats. There was also a decreased number of matured OLs (CC1<sup>+</sup>) in the ACC of TNP rats suggesting that a lack of mature OLs could account for the hypomyelination in TNP rats. We also showed decreased cells colabeling of olig2<sup>+</sup> and CC1<sup>+</sup> suggesting impairment of OPC differentiation and dramatically decreased generation of mature OLs in the ACC. Moreover, ultrastructural analysis using electron microscopy revealed that the myelin sheath thickness was compromised in TNP rats, implying that chronic ION lesion prevents OPC differentiation and impedes mature myelinating OL formation, resulting in hypomyelination.

One of the well-established functions of myelin is to modulate nerve conduction velocity (Pajevic et al., 2014). Myelin remodeling by OLs may play an important role in regulating oscillatory neuronal activity in large and complex neural networks (Chang et al., 2016; de Hoz & Simons, 2015) and facilitating the flow and integration of information (Fields, 2015). It is well known that the BLA and the ACC form an interconnected neural circuit that mediates effort-based decision-making processes (Floresco & Ghods-Sharifi, 2007). In agreement with this finding, our previous evidence suggested decreased long-term potentiation in the basolateral amygdala (BLA)-ACC synapses in rats with visceral pain (Cao, Wang, Mu, et al., 2016), and in rats after chemotherapy drug administration (Mu et al., 2015).

Furthermore, coherence and phase locking of neural spike and LFP within the ACC and between the ACC and BLA are important in the regulation of decision-making behavior in rats (Cao, Wang, Zhang, et al., 2016; Wang et al., 2017).

With regard to sensory processing, it is widely believed that cortical networks are desynchronized during active wakefulness and synchronized during quiet wakefulness and sleep (Muzur et al., 2002). In this study, we recorded the neuronal activity of the ACC within the medial PFC, defined as the cingulate cortex, area 2 (Cg2), and the prelimbic cortex with overlying cingulate cortex, area 1 (Cg1) (Gao et al., 2006), which is a major cortical area of the limbic system, integrating emotion and cognition. Specific PFC areas mediating decision-making have been discovered in brain-lesioned or psychiatric patients (Manes et al., 2002). In addition, animal studies have characterized the roles of the prelimbic, cingulate, and orbitofrontal cortices in decision-making in rats (Rivalan et al., 2009; Zeeb & Winstanley, 2013). Beyond the PFC, several studies have highlighted the role of the amygdala in advantageous decision-making in the gambling task (Bechara et al., 2003). In line with these texts, in this study we report that the synchronization of spikes in the ACC to the BLA LFP was suppressed in quiet awake rats with ION-CCI. Further, ION-CCI significantly suppressed phase locking of ACC spikes to the theta oscillations in the BLA (Figure 6). It appears that those reciprocal connections between the BLA and the ACC are critical for information transfer in this situation. These findings collectively indicate that experience has considerable impact on myelin formation and consequently enhances executive functions such as learning and memory (Fields, 2008; Hasan et al., 2019).

Oligodendroglia is a cell type that is particularly susceptible to inflammation and oxidative stress-induced excitotoxicity in both rodents and humans (Deng, 2010). Microglia contribute to the myelin plasticity through effects including the phagocytosis of myelin debris, the secretion of cytokines, chemokines, or soluble mediators at the lesion site. Reactive microglia may release various substances such as inflammatory cytokines (IL-1 $\beta$ , TNF- $\alpha$ , IL-6), NO, PGE2, ROS, and superoxide that causes damage to the neurons. Circulating cytokines may enter the CNS through diffusion or infiltration of a more permeable BBB, but they may also be released within the brain by activated glial cells (Vezzani & Viviani, 2015). We showed that higher expression of inflammatory cytokines like IL-1 $\beta$  in the ACC of TNP rats. Oligodendroglia is a cell type that is particularly susceptible to inflammation and oxidative stress-induced excitotoxicity in both rodents and humans (Deng, 2010). IL-1 $\beta$  may be cytotoxic to mature OLs causing OL cell loss but had a little effect on OPC proliferation (Takahashi et al., 2003). Inflammatory mediators activate Notch and Wnt signaling that can impede OPC differentiation causing hypomyelination.

#### 4.1 | Limitations and conclusion

Altered myelination in brain regions other than ACC has not been investigated. More studies are required to determine whether

microbial metabolites impacted myelin plasticity in chronic TNP state. Further, whether OL modification is a causal component of psychiatric phenotypes such as impaired decision-making in TNP is yet to be elucidated.

In conclusion, using a rat model of ION-CCI, we showed that chronic TNP affected TG-SpV circuitry and impaired decision-making in rats. Chronic neuropathy leads to dysregulation of myelin plasticity, and hypomyelination in ACC neuronal circuitry may disrupt brain neural signal synchrony and neural coherence, resulting in severe impact on neural network functioning.

## DECLARATION OF TRANSPARENCY

The authors, reviewers and editors affirm that in accordance to the policies set by the *Journal of Neuroscience Research*, this manuscript presents an accurate and transparent account of the study being reported and that all critical details describing the methods and results are present.

## ACKNOWLEDGMENTS

This work was supported by the Research Grants Council of Hong Kong (11100018, 11100914, 11166116, 11101315, and 160713), the National Natural Science Foundation of China (NSFC) and RGC Joint Research Scheme (3171101014, N\_CityU114/17), the Health and Medical Research Fund (05160256), and the Innovation and Technology Fund Hong Kong (CityU 9445909). This work was also supported by the City University of Hong Kong Neuroscience Research Infrastructure Grant (9610211), and Centre for Biosystems, Neuroscience, and Nanotechnology Grant (9360148).

## CONFLICT OF INTEREST

The authors declare that they have no conflict of interests.

## AUTHOR CONTRIBUTIONS

All the authors had full access to all the data in the study and take responsibility for the integrity of the data and the accuracy of the data analysis: *Conceptualization*, Y.L.; *Methodology*, Y.L. and S.K.M.; *Investigation*, S.K.M., Z.I., L.Z., M.H., Y.Z., A.S.R., and W.H.Y.; *Formal Analysis*, S.K.M., Z.I., and L.Z.; *Validation*, S.K.M., Z.I., L.Z., M.H., and Y.Z.; *Visualization*, S.K.M., Z.I., and L.Z.; *Writing – Original Draft*, Y.L. and S.K.M.; *Writing – Review & Editing*, L.Z. and A.S.R.; *Supervision*, Y.L.; *Funding Acquisition*, Y.L.

## PEER REVIEW

The peer review history for this article is available at <https://publons.com/publon/10.1002/jnr.24903>.

## DATA AVAILABILITY STATEMENT

Data available on request from the corresponding author.

## ORCID

Aruna S. Ramkrishnan  <https://orcid.org/0000-0002-8335-0510>

Ying Li  <https://orcid.org/0000-0003-3683-9695>

## REFERENCES

- Apkarian, A. V., Baliki, M. N., & Geha, P. Y. (2009). Towards a theory of chronic pain. *Progress in Neurobiology*, 87(2), 81–97. <https://doi.org/10.1016/j.pneurobio.2008.09.018>
- Apkarian, V. A., Lavarello, S., Randolph, A., Berra, H. H., Chialvo, D. R., Besedovsky, H. O., & del Rey, A. (2006). Expression of IL-1 $\beta$  in supraspinal brain regions in rats with neuropathic pain. *Neuroscience Letters*, 407(2), 176–181. <https://doi.org/10.1016/j.neulet.2006.08.034>
- Apkarian, V. A., Sosa, Y., Krauss, B. R., Thomas, S. P., Fredrickson, B. E., Levy, R. E., Harden, N. R., & Chialvo, D. R. (2004). Chronic pain patients are impaired on an emotional decision-making task. *Pain*, 108(1–2), 129–136. <https://doi.org/10.1016/j.pain.2003.12.015>
- Backonja, M. M., Coe, C. L., Muller, D. A., & Schell, K. (2008). Altered cytokine levels in the blood and cerebrospinal fluid of chronic pain patients. *Journal of Neuroimmunology*, 195(1–2), 157–163. <https://doi.org/10.1016/j.jneuroim.2008.01.005>
- Bechara, A., Damasio, H., & Damasio, A. R. (2003). Role of the amygdala in decision-making. *Annals of the New York Academy of Sciences*, 985, 356–369. <https://doi.org/10.1111/j.1749-6632.2003.tb07094.x>
- Bechara, A., Damasio, H., Tranel, D., & Damasio, A. R. (1997). Deciding advantageously before knowing the advantageous strategy. *Science*, 275(5304), 1293–1295. <https://doi.org/10.1126/science.275.5304.1293>
- Bechara, A., Tranel, D., & Damasio, H. (2000). Characterization of the decision-making deficit of patients with ventromedial prefrontal cortex lesions. *Brain*, 123(11), 2189–2202. <https://doi.org/10.1093/brain/123.11.2189>
- Bliss, T. V., Collingridge, G. L., Kaang, B. K., & Zhuo, M. (2016). Synaptic plasticity in the anterior cingulate cortex in acute and chronic pain. *Nature Reviews Neuroscience*, 17(8), 485–496. <https://doi.org/10.1038/nrn.2016.68>
- Borsook, D., DaSilva, A. F., Ploghaus, A., & Becerra, L. (2003). Specific and somatotopic functional magnetic resonance imaging activation in the trigeminal ganglion by brush and noxious heat. *Journal of Neuroscience*, 23(21), 7897–7903. <https://doi.org/10.1523/jneurosci.23-21-07897.2003>
- Buzsáki, G., & Draguhn, A. (2004). Neuronal oscillations in cortical networks. *Science*, 304(5679), 1926–1929. <https://doi.org/10.1126/science.1099745>
- Cao, B., Wang, J., Mu, L., Poon, D., & Li, Y. (2016). Impairment of decision making associated with disruption of phase-locking in the anterior cingulate cortex in viscerally hypersensitive rats. *Experimental Neurology*, 286, 21–31. <https://doi.org/10.1016/j.expneurol.2016.09.010>
- Cao, B., Wang, J., Shahed, M., Jelfs, B., Chan, R. H., & Li, Y. (2016). Vagus nerve stimulation alters phase synchrony of the anterior cingulate cortex and facilitates decision making in rats. *Scientific Reports*, 6, 35135. <https://doi.org/10.1038/srep35135>
- Cao, B., Wang, J., Zhang, X. U., Yang, X., Poon, D.-H., Jelfs, B., Chan, R. H. M., Wu, J.-Y., & Li, Y. (2016). Impairment of decision making and disruption of synchrony between basolateral amygdala and anterior cingulate cortex in the maternally separated rat. *Neurobiology of Learning and Memory*, 136, 74–85. <https://doi.org/10.1016/j.nlm.2016.09.015>
- Cao, Z., Wu, X., Chen, S., Fan, J., Zhang, R., Owyang, C., & Li, Y. (2008). Anterior cingulate cortex modulates visceral pain as measured by visceromotor responses in viscerally hypersensitive rats. *Gastroenterology*, 134(2), 535–543. <https://doi.org/10.1053/j.gastro.2007.11.057>
- Chang, K. J., Redmond, S. A., & Chan, J. R. (2016). Remodeling myelination: Implications for mechanisms of neural plasticity. *Nature Neuroscience*, 19(2), 190–197. <https://doi.org/10.1038/nn.4200>

- Colgin, L. L. (2013). Mechanisms and functions of theta rhythms. *Annual Review of Neuroscience*, 36, 295–312. <https://doi.org/10.1146/annurev-neuro-062012-170330>
- Costa, G. M. F., de Oliveira, A. P., Martinelli, P. M., da Silva Camargos, E. R., Arantes, R. M. E., & de Almeida-Leite, C. M. (2016). Demyelination/remyelination and expression of interleukin-1 $\beta$ , substance P, nerve growth factor, and glial-derived neurotrophic factor during trigeminal neuropathic pain in rats. *Neuroscience Letters*, 612, 210–218. <https://doi.org/10.1016/j.neulet.2015.12.017>
- Davis, K. D., Hutchison, W. D., Lozano, A. M., & Dostrovsky, J. O. (1994). Altered pain and temperature perception following cingulotomy and capsulotomy in a patient with schizoaffective disorder. *Pain*, 59(2), 189–199. [https://doi.org/10.1016/0304-3959\(94\)90071-x](https://doi.org/10.1016/0304-3959(94)90071-x)
- de Hoz, L., & Simons, M. (2015). The emerging functions of oligodendrocytes in regulating neuronal network behaviour. *BioEssays*, 37(1), 60–69. <https://doi.org/10.1002/bies.201400127>
- Deng, W. (2010). Neurobiology of injury to the developing brain. *Nature Reviews. Neurology*, 6(6), 328–336. <https://doi.org/10.1038/nrneuro.2010.53>
- Düzel, E., Penny, W. D., & Burgess, N. (2010). Brain oscillations and memory. *Current Opinion in Neurobiology*, 20(2), 143–149. <https://doi.org/10.1016/j.conb.2010.01.004>
- Fan, J., Wu, X., Cao, Z., Chen, S., Owyang, C., & Li, Y. (2009). Up-regulation of anterior cingulate cortex NR2B receptors contributes to visceral pain responses in rats. *Gastroenterology*, 136(5), 1732–1740. <https://doi.org/10.1053/j.gastro.2009.01.069>
- Fields, R. D. (2008). White matter in learning, cognition and psychiatric disorders. *Trends in Neurosciences*, 31(7), 361–370. <https://doi.org/10.1016/j.tins.2008.04.001>
- Fields, R. D. (2015). A new mechanism of nervous system plasticity: Activity-dependent myelination. *Nature Reviews Neuroscience*, 16(12), 756–767. <https://doi.org/10.1038/nrn4023>
- Floresco, S. B., & Ghods-Sharifi, S. (2007). Amygdala-prefrontal cortical circuitry regulates effort-based decision making. *Cerebral Cortex*, 17(2), 251–260. <https://doi.org/10.1093/cercor/bhj143>
- Gao, J., Wu, X., Owyang, C., & Li, Y. (2006). Enhanced responses of the anterior cingulate cortex neurones to colonic distension in viscerally hypersensitive rats. *Journal of Physiology*, 570(Pt 1), 169–183. <https://doi.org/10.1113/jphysiol.2005.096073>
- Hart, R. P., Martelli, M. F., & Zasler, N. D. (2000). Chronic pain and neuropsychological functioning. *Neuropsychology Review*, 10(3), 131–149. <https://doi.org/10.1023/a:1009020914358>
- Hasan, M., Kanna, M. S., Jun, W., Ramkrishnan, A. S., Iqbal, Z., Lee, Y., & Li, Y. (2019). Schema-like learning and memory consolidation acting through myelination. *The FASEB Journal*, 33(11), 11758–11775. <https://doi.org/10.1096/fj.201900910R>
- Hill, R. A., Li, A. M., & Grutzendler, J. (2018). Lifelong cortical myelin plasticity and age-related degeneration in the live mammalian brain. *Nature Neuroscience*, 21(5), 683–695. <https://doi.org/10.1038/s41593-018-0120-6>
- Hossaini, M., Jongen, J. L. M., Biesheuvel, K., Kuhl, D., & Holstege, J. C. (2010). Nociceptive stimulation induces expression of Arc/Arg3.1 in the spinal cord with a preference for neurons containing enkephalin. *Molecular Pain*, 6, 43. <https://doi.org/10.1186/1744-8069-6-43>
- Hu, H. (2016). Reward and aversion. *Annual Review of Neuroscience*, 39, 297–324. <https://doi.org/10.1146/annurev-neuro-070815-014106>
- Hu, H., Cui, Y., & Yang, Y. (2020). Circuits and functions of the lateral habenula in health and in disease. *Nature Reviews Neuroscience*, 21(5), 277–295. <https://doi.org/10.1038/s41583-020-0292-4>
- Hutchison, W. D., Davis, K. D., Lozano, A. M., Tasker, R. R., & Dostrovsky, J. O. (1999). Pain-related neurons in the human cingulate cortex. *Nature Neuroscience*, 2(5), 403–405. <https://doi.org/10.1038/8065>
- Iwata, K., Miyachi, S., Imanishi, M., Tsuboi, Y., Kitagawa, J., Teramoto, K., Hitomi, S., Shinoda, M., Kondo, M., & Takada, M. (2011). Ascending multisynaptic pathways from the trigeminal ganglion to the anterior cingulate cortex. *Experimental Neurology*, 227(1), 69–78. <https://doi.org/10.1016/j.expneurol.2010.09.013>
- Kayser, V., Viguier, F., Ioannidi, M., Bernard, J.-F., Latrémolière, A., Michot, B., Vela, J.-M., Buschmann, H., Hamon, M., & Bourgoin, S. (2010). Differential anti-neuropathic pain effects of tetrodotoxin in sciatic nerve- versus infraorbital nerve-ligated rats—behavioral, pharmacological and immunohistochemical investigations. *Neuropharmacology*, 58(2), 474–487. <https://doi.org/10.1016/j.neuropharm.2009.09.003>
- Kernisant, M., Gear, R. W., Jasmin, L., Vit, J. P., & Ohara, P. T. (2008). Chronic constriction injury of the infraorbital nerve in the rat using modified syringe needle. *Journal of Neuroscience Methods*, 172(1), 43–47. <https://doi.org/10.1016/j.jneumeth.2008.04.013>
- Kim, S. K., & Nabekura, J. (2011). Rapid synaptic remodeling in the adult somatosensory cortex following peripheral nerve injury and its association with neuropathic pain. *Journal of Neuroscience*, 31(14), 5477–5482. <https://doi.org/10.1523/jneurosci.0328-11.2011>
- Latremoliere, A., & Woolf, C. J. (2009). Central sensitization: A generator of pain hypersensitivity by central neural plasticity. *Journal of Pain: Official Journal of the American Pain Society*, 10(9), 895–926. <https://doi.org/10.1016/j.jpain.2009.06.012>
- Leite-Almeida, H., Guimarães, M. R., Cerqueira, J. J., Ribeiro-Costa, N., Anjos-Martins, H., Sousa, N., & Almeida, A. (2014). Asymmetric c-Fos expression in the ventral orbital cortex is associated with impaired reversal learning in a right-sided neuropathy. *Molecular Pain*, 10, 41. <https://doi.org/10.1186/1744-8069-10-41>
- Li, X. Y., Ko, H. G., Chen, T., Descalzi, G., Koga, K., Wang, H., Kim, S. S., Shang, Y., Kwak, C., Park, S. W., Shim, J., Lee, K., Collingridge, G. L., Kaang, B. K., & Zhuo, M. (2010). Alleviating neuropathic pain hypersensitivity by inhibiting PKMzeta in the anterior cingulate cortex. *Science*, 330(6009), 1400–1404. <https://doi.org/10.1126/science.119792>
- Li, X., Zhao, Z., Ma, J., Cui, S., Yi, M., Guo, H., & Wan, Y. (2017). Extracting neural oscillation signatures of laser-induced nociception in pain-related regions in rats. *Frontiers in Neural Circuits*, 11, 71. <https://doi.org/10.3389/fncir.2017.00071>
- Lu, Y. I., Zhong, C., Wang, L., Wei, P., He, W., Huang, K., Zhang, Y. I., Zhan, Y., Feng, G., & Wang, L. (2016). Optogenetic dissection of ictal propagation in the hippocampal-entorhinal cortex structures. *Nature Communications*, 7(1), 10962. <https://doi.org/10.1038/ncomms10962>
- Manes, F., Sahakian, B., Clark, L., Rogers, R., Antoun, N., Aitken, M., & Robbins, T. (2002). Decision-making processes following damage to the prefrontal cortex. *Brain*, 125(Pt 3), 624–639. <https://doi.org/10.1093/brain/awf049>
- Marbach, J. J. (1993). Is phantom tooth pain a deafferentation (neuropathic) syndrome? Part I: Evidence derived from pathophysiology and treatment. *Oral Surgery, Oral Medicine, Oral Pathology*, 75(1), 95–105. [https://doi.org/10.1016/0030-4220\(93\)90413-x](https://doi.org/10.1016/0030-4220(93)90413-x)
- Markram, H., Lübke, J., Frotscher, M., & Sakmann, B. (1997). Regulation of synaptic efficacy by coincidence of postsynaptic APs and EPSPs. *Science*, 275(5297), 213–215. <https://doi.org/10.1126/science.275.5297.213>
- May, A. (2008). Chronic pain may change the structure of the brain. *Pain*, 137(1), 7–15. <https://doi.org/10.1016/j.pain.2008.02.034>
- McKenzie, I. A., Ohayon, D., Li, H., de Faria, J. P., Emery, B., Tohyama, K., & Richardson, W. D. (2014). Motor skill learning requires active central myelination. *Science*, 346(6207), 318–322. <https://doi.org/10.1126/science.1254960>
- Mu, L. I., Wang, J., Cao, B., Jelfs, B., Chan, R. H. M., Xu, X., Hasan, M., Zhang, X. U., & Li, Y. (2015). Impairment of cognitive function by chemotherapy: Association with the disruption of phase-locking and synchronization in anterior cingulate cortex. *Molecular Brain*, 8, 32. <https://doi.org/10.1186/s13041-015-0125-y>
- Muzur, A., Pace-Schott, E. F., & Hobson, J. A. (2002). The prefrontal cortex in sleep. *Trends in Cognitive Sciences*, 6(11), 475–481. [https://doi.org/10.1016/s1364-6613\(02\)01992-7](https://doi.org/10.1016/s1364-6613(02)01992-7)

- Pajevic, S., Basser, P. J., & Fields, R. D. (2014). Role of myelin plasticity in oscillations and synchrony of neuronal activity. *Neuroscience*, 276, 135–147. <https://doi.org/10.1016/j.neuroscience.2013.11.007>
- Paulus, M. P. (2007). Decision-making dysfunctions in psychiatry—altered homeostatic processing? *Science*, 318(5850), 602–606. <https://doi.org/10.1126/science.1142997>
- Rahman, S., Sahakian, B. J., Cardinal, R. N., Rogers, R. D., & Robbins, T. W. (2001). Decision making and neuropsychiatry. *Trends in Cognitive Sciences*, 5(6), 271–277. [https://doi.org/10.1016/S1364-6613\(00\)01650-8](https://doi.org/10.1016/S1364-6613(00)01650-8)
- Rivalan, M., Ahmed, S. H., & Dellu-Hagedorn, F. (2009). Risk-prone individuals prefer the wrong options on a rat version of the Iowa Gambling Task. *Biological Psychiatry*, 66(8), 743–749. <https://doi.org/10.1016/j.biopsych.2009.04.008>
- Rutishauser, U., Ross, I. B., Mamelak, A. N., & Schuman, E. M. (2010). Human memory strength is predicted by theta-frequency phase-locking of single neurons. *Nature*, 464(7290), 903–907. <https://doi.org/10.1038/nature08860>
- Sessle, B. (2005). Trigeminal central sensitization. *Reviews in Analgesia*, 8, 85–102. <https://doi.org/10.3727/000000005783992881>
- Shidara, M., & Richmond, B. J. (2002). Anterior cingulate: Single neuronal signals related to degree of reward expectancy. *Science*, 296(5573), 1709–1711. <https://doi.org/10.1126/science.1069504>
- Takahashi, J. L., Giuliani, F., Power, C., Imai, Y., & Yong, V. W. (2003). Interleukin-1 $\beta$  promotes oligodendrocyte death through glutamate excitotoxicity. *Annals of Neurology*, 53(5), 588–595. <https://doi.org/10.1002/ana.10519>
- Talbot, J. D., Marrett, S., Evans, A. C., Meyer, E., Bushnell, M. C., & Duncan, G. H. (1991). Multiple representations of pain in human cerebral cortex. *Science*, 251(4999), 1355–1358. <https://doi.org/10.1126/science.2003220>
- Thion, M. S., Ginhoux, F., & Garel, S. (2018). Microglia and early brain development: An intimate journey. *Science*, 362(6411), 185–189. <https://doi.org/10.1126/science.aat0474>
- Varela, F., Lachaux, J.-P., Rodriguez, E., & Martinerie, J. (2001). The brainweb: Phase synchronization and large-scale integration. *Nature Reviews Neuroscience*, 2(4), 229–239. <https://doi.org/10.1038/35067550>
- Vezzani, A., & Viviani, B. (2015). Neuromodulatory properties of inflammatory cytokines and their impact on neuronal excitability. *Neuropharmacology*, 96(Pt A), 70–82. <https://doi.org/10.1016/j.neuropharm.2014.10.027>
- Vogt, B. A., Sikes, R. W., & Vogt, L. J. (1993). Anterior cingulate cortex and the medial pain system. In B. A. Vogt & M. Gabriel (Eds.), *Neurobiology of cingulate cortex and limbic thalamus: A comprehensive handbook* (pp. 313–344). Birkhäuser.
- Vos, B. P., Strassman, A. M., & Maciewicz, R. J. (1994). Behavioral evidence of trigeminal neuropathic pain following chronic constriction injury to the rat's infraorbital nerve. *Journal of Neuroscience*, 14(5 Pt 1), 2708–2723. <https://doi.org/10.1523/jneurosci.14-05-02708.1994>
- Wang, J., Tu, J., Cao, B., Mu, L. I., Yang, X., Cong, M. I., Ramkrishnan, A. S., Chan, R. H. M., Wang, L., & Li, Y. (2017). Astrocytic l-lactate signaling facilitates amygdala-anterior cingulate cortex synchrony and decision making in rats. *Cell Reports*, 21(9), 2407–2418. <https://doi.org/10.1016/j.celrep.2017.11.012>
- Wang, J., Zhang, X., Cao, B., Liu, J., & Li, Y. (2015). Facilitation of synaptic transmission in the anterior cingulate cortex in viscerally hypersensitive rats. *Cerebral Cortex*, 25(4), 859–868. <https://doi.org/10.1093/cercor/bht273>
- Willoch, F., Gamringer, U., Medele, R., Steude, U., & Tölle, T. R. (2003). Analgesia by electrostimulation of the trigeminal ganglion in patients with trigeminopathic pain: A PET activation study. *Pain*, 103(1), 119–130. [https://doi.org/10.1016/s0304-3959\(02\)00423-2](https://doi.org/10.1016/s0304-3959(02)00423-2)
- Witting, N., Kupers, R. C., Svensson, P., & Jensen, T. S. (2006). A PET activation study of brush-evoked allodynia in patients with nerve injury pain. *Pain*, 120(1–2), 145–154. <https://doi.org/10.1016/j.pain.2005.10.034>
- Wu, X., Gao, J., Yan, J., Fan, J., Owyang, C., & Li, Y. (2008). Role for NMDA receptors in visceral nociceptive transmission in the anterior cingulate cortex of viscerally hypersensitive rats. *American Journal of Physiology. Gastrointestinal and Liver Physiology*, 294(4), G918–G927. <https://doi.org/10.1152/ajpgi.00452.2007>
- Xiao, L., Ohayon, D., McKenzie, I. A., Sinclair-Wilson, A., Wright, J. L., Fudge, A. D., Emery, B., Li, H., & Richardson, W. D. (2016). Rapid production of new oligodendrocytes is required in the earliest stages of motor-skill learning. *Nature Neuroscience*, 19(9), 1210–1217. <https://doi.org/10.1038/nn.4351>
- Xie, W., Luo, S., Xuan, H., Chou, C., Song, G., Lv, R., Jin, Y., Li, W., & Xu, J. (2006). Betamethasone affects cerebral expressions of NF-kappaB and cytokines that correlate with pain behavior in a rat model of neuropathy. *Annals of Clinical and Laboratory Science*, 36(1), 39–46.
- Xin, W., & Chan, J. R. (2020). Myelin plasticity: Sculpting circuits in learning and memory. *Nature Reviews Neuroscience*, 21, 682–694. <https://doi.org/10.1038/s41583-020-00379-8>
- Yan, N., Cao, B., Xu, J., Hao, C., Zhang, X., & Li, Y. (2012). Glutamatergic activation of anterior cingulate cortex mediates the affective component of visceral pain memory in rats. *Neurobiology of Learning and Memory*, 97(1), 156–164. <https://doi.org/10.1016/j.nlm.2011.11.003>
- Zatorre, R. J., Fields, R. D., & Johansen-Berg, H. (2012). Plasticity in gray and white: Neuroimaging changes in brain structure during learning. *Nature Neuroscience*, 15(4), 528–536. <https://doi.org/10.1038/nn.3045>
- Zeeb, F. D., & Winstanley, C. A. (2013). Functional disconnection of the orbitofrontal cortex and basolateral amygdala impairs acquisition of a rat gambling task and disrupts animals' ability to alter decision-making behavior after reinforcer devaluation. *Journal of Neuroscience*, 33(15), 6434–6443. <https://doi.org/10.1523/JNEUROSCI.3971-12.2013>
- Zhuo, M. (2019). Long-term cortical synaptic changes contribute to chronic pain and emotional disorders. *Neuroscience Letters*, 702, 66–70. <https://doi.org/10.1016/j.neulet.2018.11.048>

## SUPPORTING INFORMATION

Additional Supporting Information may be found online in the Supporting Information section.

**FIGURE S1.** Unprocessed Western blot images for Figure 8B. (a) Unprocessed Western blot image of MBP protein band, (b) Unprocessed Western blot image of  $\beta$ -Actin protein band

**FIGURE S2.** Unprocessed western blot images for Figure 10A. (a) Unprocessed Western blot image of  $\beta$ -Actin protein band, (b) Unprocessed Western blot image of CD68 protein band, (c) Unprocessed Western blot image of IL-1  $\beta$  protein band

Transparent Peer Review Report

Transparent Science Questionnaire for Authors

**How to cite this article:** Murugappan, S. K., Hasan M., Lei Z., Iqbal Z., Ramkrishnan A. S., Wong H. Y., & Li Y. (2021).

Trigeminal neuropathy causes hypomyelination in the anterior cingulate cortex, disrupts the synchrony of neural circuitry, and impairs decision-making in male rats. *Journal of Neuroscience Research*, 99, 2721–2742. <https://doi.org/10.1002/jnr.24903>